Arctic atmospheric mercury

Dastoor, Ashu; Wilson, Simon J.; Travnikov, Oleg; Ryjkov, Andrei; Angot, Hélène; Christensen, Jesper H.; Steenhuisen, Frits; Muntean, Marilena

Published in:
The Science of the Total Environment

DOI:
10.1016/j.scitotenv.2022.156213

Publication date:
2022

Science of the Total Environment 839 (2022) 156213

Contents lists available at ScienceDirect

Science of the Total Environment

journal homepage: www.elsevier.com/locate/scitotenv

Arctic atmospheric mercury: Sources and changes

Ashu Dastoor [a,*], Simon J. Wilson [b,*], Oleg Travnikov [c], Andrei Ryjkov [a], Hélène Angot [d], Jesper H. Christensen [e], Frits Steenhuisen [f], Marilena Muntean [g]

[a] Air Quality Research Division, Environment and Climate Change Canada, 2121 Trans-Canada Highway, Dorval, Québec H9P 1J3, Canada
[b] Arctic Monitoring and Assessment Programme (AMAP). The Fram Centre, Box 6606 Stakkevollan, 9296 Tromsø, Norway
[c] Meteorological Synthesizing Centre-East, EMEP, 2nd Roshchinsky proezd, 8/5, 115419 Moscow, Russia
[d] Extreme Environments Research Laboratory, École Polytechnique Fédérale de Lausanne (EPFL) Valais Wallis, Sion, Switzerland
[e] Department of Environmental Science, iClimate, Aarhus University, Frederiksborgvej 399, 4000 Roskilde, Denmark
[f] Arctic Centre, University of Groningen, Aweg 30, 9718CW Groningen, the Netherlands
[g] European Commission, Joint Research Centre (JRC), Via E. Fermi 2749 (T.P. 123), I-21027 Ispra, VA, Italy

HIGHLIGHTS

- Emission inventories need regular/consistent updating with improved Hg speciation.
- Models confirm important impact of changing meteorology on Arctic atmospheric Hg.
- 75% of anthropogenic Hg deposition is from industrial and ASGM gold mining sources.
- Significant geographic and seasonal variations exist in Arctic Hg contamination.
- Geographical distribution of air monitoring needs improvement to capture changes.

GRAPHICAL ABSTRACT

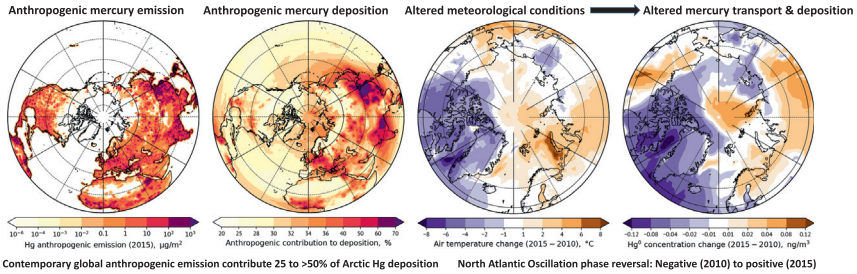

ARTICLE INFO

Editor: Zhouqing Xie

Keywords:
Emissions
Anthropogenic
Transport
Deposition
Modeling
Attribution

ABSTRACT

Global anthropogenic and legacy mercury (Hg) emissions are the main sources of Arctic Hg contamination, primarily transported there via the atmosphere. This review summarizes the state of knowledge of the global anthropogenic sources of Hg emissions, and examines recent changes and source attribution of Hg transport and deposition to the Arctic using models. Estimated global anthropogenic Hg emissions to the atmosphere for 2015 were ~2220 Mg, ~20% higher than 2010. Global anthropogenic, legacy and geogenic Hg emissions were, respectively, responsible for 32%, 64% (wildfires: 6–10%) and 4% of the annual Arctic Hg deposition. Relative contributions to Arctic deposition of anthropogenic origin was dominated by sources in East Asia (32%), Commonwealth of Independent States (12%), and Africa (12%). Model results exhibit significant spatiotemporal variations in Arctic anthropogenic Hg deposition fluxes, driven by regional differences in Hg air transport routes, surface and precipitation uptake rates, and interseasonal differences in atmospheric circulation and deposition pathways. Model simulations reveal that changes in meteorology are having a profound impact on contemporary atmospheric Hg in the Arctic. Reversal of North Atlantic Oscillation phase from strongly negative in 2010 to positive in 2015, associated with lower temperature and more sea ice in the Canadian Arctic, Greenland and surrounding ocean, resulted in enhanced production of bromine species and Hg(0) oxidation and lower evasion of Hg(0) from ocean waters in 2015. This led to increased Hg(II) (and its deposition) and reduced Hg(0) air concentrations in these regions in line with High Arctic observations. However, combined changes in meteorology and anthropogenic emissions led to overall elevated modeled Arctic air Hg(0) levels in 2015 compared to 2010 contrary to observed declines at most monitoring sites, likely due to uncertainties in anthropogenic emission speciation, wildfire emissions and model representations of air-surface Hg fluxes.

* Corresponding authors.
E-mail addresses: ashu.dastoor@ec.gc.ca (A. Dastoor), simon.wilson@amap.no (S.J. Wilson).

http://dx.doi.org/10.1016/j.scitotenv.2022.156213
Received 1 March 2022; Received in revised form 17 May 2022; Accepted 20 May 2022
Available online 24 May 2022

1. Introduction

Mercury (Hg) is emitted to the atmosphere from both anthropogenic and natural sources in inorganic form; it then circulates and accumulates in global environments through a series of complex physicochemical processes involving transport, physico-chemical transformations, and air-surface exchanges on a global scale and within the Arctic (AMAP, 2011). Dastoor et al. (2022) presented a comprehensive review of the present-day total Hg mass balance (Hg levels, fluxes, and reservoir budgets) in the Arctic. Identifying the origin of mercury in the Arctic environment is central to addressing policy to reduce Arctic mercury contamination. Action to reduce present-day anthropogenic Hg emissions and releases, through for example the *Minamata Convention on Mercury*, is the key to reducing the further accumulation of Hg in environmental media and future re-emissions of Hg (Schartup et al., 2022). Given the vulnerability of Arctic populations to mercury pollution, monitoring and assessment of mercury levels and their trends in the region are of particular interest to the *Convention* in the context of effectiveness evaluation. The effects of profound shifts in the climate and the cryosphere in warming Arctic (AMAP, 2019; Box et al., 2019; Saros et al., 2019) are complex because of potential interactive alterations to multiple processes including Hg transport and surface exchanges (Chételat et al., 2022), and biogeochemical transformations (MacMillan et al., 2015; Yang et al., 2016). In addition, climate change impacts vary across the Arctic, due to regional differences in warming, sea-ice loss, and snow cover changes (AMAP, 2017). Considerations of these effects on atmospheric Hg transport, transformation, and deposition are warranted to assess the impacts of concurrent changes in climate and emissions on Hg cycling. While monitoring data show the combined impact of changes in multiple factors affecting Hg cycling such as anthropogenic emissions, land use, environmental chemical composition, and climate, evaluating the effectiveness of the *Convention* entails isolating the impacts attributable to the *Convention* from changes occurring due to other factors. Mechanistic models can be used to resolve the intervening Hg processes and help quantitatively attribute mercury levels and their temporal trends to different sources and drivers. Reliable time-varying inputs of anthropogenic emissions of Hg species from global source regions are necessary to simulate mercury levels and their changes accurately using the atmospheric models.

This review is a contribution to the Virtual Special Issue on the AMAP Assessment 2021: Mercury in the Arctic (AMAP, 2021). It presents the development of the most recent (2015) global inventory of anthropogenic Hg emissions to air (that contribute to Hg contamination globally and in the Arctic). Mercury enters the Arctic environment via the atmosphere, ocean currents, and river runoff. Hg observations in Arctic environments are scarce due to the challenges associated with the size and remoteness of the region. However, since the previous AMAP mercury assessment (AMAP, 2011), major measurements campaigns and new analytical techniques have elucidated Hg pathways with greater clarity. Advances have been made in the understanding of Hg chemistry (Dibble et al., 2020), and flux exchange processes with vegetation (Obrist et al., 2017), snowpack (Douglas et al., 2017), and marine surfaces (DiMento et al., 2019). Based on these advances, process representations in Hg models have been improved (Angot et al., 2016; Zhou et al., 2021), reducing uncertainties in estimates of Hg transport and deposition in the Arctic. Using updated global Hg models, Hg transport and deposition in the Arctic was simulated based on 2015 AMAP/UN-Environment anthropogenic emissions (AMAP/UNEP, 2019).

In order to assess the impact of global sources of Hg emission on contemporary Hg levels in Arctic ecosystems, we review here the state of knowledge and understanding of the global sources of Hg emissions to the atmosphere, and Arctic Hg transport and levels and their changes and source attribution using Hg models. A review of observed Hg trends and their long-term changes in Arctic atmosphere due to climate change influences are presented separately in this special issue (Chételat et al., 2022; MacSween et al., 2022). Long-term trends in global atmospheric Hg emissions and associated model simulated atmospheric Hg levels in the Arctic are not addressed due to inconsistencies in available datasets representing global anthropogenic Hg emission trends and their spatial distribution. However, the models were applied to simulate recent changes in atmospheric Hg levels (2010 to 2015) to develop an insight into the drivers for changes in Arctic atmospheric Hg between these two years, including not only changes that might occur related to changing anthropogenic emissions, but also those directly and indirectly associated with climate warming. Next, the attribution of atmospheric Hg deposition to specific sources such as primary anthropogenic and legacy mercury emissions as well as the relative importance of local sources vs. global sources was determined using the model ensemble. Finally, conclusions and recommendations are provided for future evaluation of atmospheric Hg sources, levels, and their changes in the Arctic.

2. Sources of mercury emissions to air contributing to mercury in Arctic environments

Evidence of a notable increase in present-day Hg concentrations in Arctic environments compared to pre-industrial levels and the lack of any significant anthropogenic mercury emissions sources within the Arctic region itself implies that the majority of Hg contaminating the Arctic environment originates from sources outside the Arctic (Dietz et al., 2009; AMAP, 2011). Long-range transport via air, oceans, and rivers is therefore the dominant means by which mercury is delivered to, and contaminates the Arctic environment and its ecosystems (AMAP, 1998, 2005, 2011; Dastoor et al., 2022). The atmospheric pathway is particularly important in this respect.

The main species of Hg emitted to the atmosphere, gaseous elemental mercury (Hg(0); GEM), has a long lifetime in the air (0.5–1 year; Horowitz et al., 2017), which transports and deposits on a global scale. Additionally, Hg(0) reacts with strong oxidants in air, and forms oxidized mercury species (Hg(II): gaseous oxidized mercury (GOM) and particulate bound mercury (PBM)) that readily deposit to global ecosystems by direct uptake and precipitation scavenging on a shorter time-scale (up to two weeks). In coastal and marine Arctic environments, Hg oxidation and deposition processes intensify during springtime, facilitated by increased photochemical production of bromine (Br) species from snowpacks over sea ice (Moore et al., 2014; Toyota et al., 2014a; Wang et al., 2019). The resulting Arctic mercury depletion events (AMDEs) enhance the net deposition of mercury in springtime in areas where AMDEs occur. Due to its volatile nature, a fraction of historically deposited Hg reenters the atmosphere from earth's surfaces, significantly amplifying environmental Hg circulation and transport to the Arctic through the process of global fractionation. Burial in long-term storage archives such as lake sediments, ocean sediments, subsurface soils, and glacial ice ultimately immobilizes Hg from its circulation in global environments.

The Global Mercury Assessment 2018 (AMAP/UNEP, 2019) included an updated global Hg budget (Outridge et al., 2018) that estimates present-day global emissions of Hg to air at approximately 8000 Mg yr^{-1} (4600 Mg yr^{-1} and 3400 Mg yr^{-1} from terrestrial and marine sources, respectively). These emissions originate from the following sources: ~500 Mg yr^{-1} from natural (geogenic) sources; ~1600 Mg yr^{-1} from re-emissions from the soil, vegetation, and open biomass burning; ~3400 Mg yr^{-1} from evasion from surface ocean waters; and ~ 2500 Mg yr^{-1} from anthropogenic sources. The atmosphere is estimated to hold ~4400 Mg of Hg, representing a percentage increase due to human activities of ~450% since around the mid-15th century. The average global mercury emissions by wildfires have been estimated in the range of 400 to 675 Mg yr^{-1} (Friedli et al., 2009; De Simone et al., 2017; Kumar et al., 2018). The global budget also includes an estimate of ~600 Mg of Hg released to freshwater aquatic environments in 2015 from anthropogenic sources; this amount does not include releases associated with artisanal and small-scale gold mining (ASGM) activities, which are estimated to contribute ~1200 Mg of Hg in combined releases to land and water in 2015 (AMAP/UNEP, 2019; Kocman et al., 2017). ASGM-associated releases to water are additional to the significant contribution that this sector makes to emissions of Hg to air.

Current annual emissions to air from anthropogenic sources (contributing ~30% of total Hg emissions) and natural sources (contributing <10%) are substantially lower than re-emissions/evasion from soils/vegetation and surface ocean waters, which together contribute ~60% of total Hg emissions. However, it should be recognized that the re-emissions—essentially a result of natural processes—are themselves largely a consequence of the build-up of Hg in the environment following historical anthropogenic emissions and releases. In the context of the budget, emissions from Hg released or disposed of to land (e.g., landfill, mine tailings, and waste rock, etc.) are also treated as re-emission sources. Action to reduce present-day anthropogenic Hg emissions and releases (through, for example, the global Minamata Convention on Mercury) is, therefore, the key to reducing the further accumulation of Hg in environmental media and future re-emissions of Hg (see Schartup et al., 2022).

Due to the sparse population and limited human activities in the Arctic, natural emissions (geogenic and legacy (from previously deposited) emissions including wildfire emissions) within the Arctic also play an important role in the region. Combined geogenic and re-emissions of Hg from soils/vegetation and marine surfaces in the Arctic are estimated in the range of 7 to 59 Mg yr^{-1} (median: 24 Mg yr^{-1}) and 23 to 45 Mg yr^{-1} (median: 32 Mg yr^{-1}), respectively (Dastoor et al., 2022). Arctic soils have been found to be long-term storage for a large amount of Hg (Schuster et al., 2018), and releases of legacy Hg stored in boreal forests (Jiskra et al., 2018) and soils can be significant under large-scale fire events. Kumar et al. (2018) estimated that around 95% of Hg wildfire emissions in the Arctic are from boreal forests and 5% are from other vegetation types. Emissions estimates from boreal forest fires range from ~20 Mg yr^{-1} (McLagan et al., 2021; Friedli et al., 2003a) up to 200 Mg yr^{-1} (Kumar et al., 2018). Recently, Dastoor et al. (2022) estimated mean wildfire Hg emissions north of 60°N at 8.8 ± 6.4 Mg yr^{-1} (2001 to 2019) based on the mean burned area (Giglio et al., 2013, 2016; Lizundia-Loiola et al., 2020), the mean fuel load of Canadian Arctic biomes (Amiro et al., 2001), and the emission factors based on McLagan et al. (2021).

Uncertainties in Hg re-emission estimates are high due to a lack of observed air-surface flux estimates representing all surface types and seasons. Increased melting of permafrost, glaciers, and ice sheets in the Arctic over the last decades is suggested to be releasing Hg into the Arctic environment (Milner et al., 2017; Schuster et al., 2018), but estimates of air emissions from these sources are currently lacking (Schaefer et al., 2020). Wildfire emission uncertainties are associated with the estimation of annual burned area and emission factors, limited near-source atmospheric Hg measurements in wildfire plumes (Friedli et al., 2009; De Simone et al., 2017; McLagan et al., 2021), and lack of speciated wildfire emission inventories (Friedli et al., 2003; Finley et al., 2009; Kohlenberg et al., 2018; Fraser et al., 2018). Peatlands are an important sink for organic matter and Hg in the circumboreal regions, and the burning of peat-rich soils likely leads to a significantly greater release of Hg than is currently estimated (Turetsky et al., 2006; Fraser et al., 2018). Fire frequency, intensity and length of the burning season are expected to increase in the future under warming conditions and might lead to higher wildfire Hg emissions (Mack et al., 2011; Veira et al., 2016; Walker et al., 2019).

The following sections provide estimates of anthropogenic emissions of Hg relevant to Arctic Hg contamination. The anthropogenic emissions for 2015 described here were used to simulate present-day geospatial distributions of Hg levels in the Arctic air and deposition, and to determine the source apportionment of Hg deposition using multiple models.

2.1. Anthropogenic emissions

2.1.1. Global anthropogenic emissions in 2015

Due to the significance of long-range transport from sources remote to the Arctic, mercury assessments prepared under the auspices of the AMAP over the past 3 decades have included consideration of global emissions of mercury. An important contribution to this work involved the construction of global inventories of anthropogenic mercury emissions to air, their spatial distribution, and modeling of global atmospheric transport in order to investigate source-receptor relationships to inform policy aimed at reducing Arctic mercury contamination. As part of the AMAP, 2011 and 2021 mercury assessment cycles, this emission inventory work was undertaken by joint AMAP/UNEP expert groups to provide technical input also to UN Global Mercury Assessments (GMA; UNEP, 2013; UNEP, 2019). The most recent AMAP/UNEP global inventory of Hg emissions to air from anthropogenic sources is for 2015, building on earlier AMAP global anthropogenic emissions inventory work reported in AMAP mercury assessments (AMAP, 1998, 2005, 2011; Pacyna and Pacyna, 2002; Pacyna et al., 2006, 2010) and applying a revised methodological approach that was introduced in preparing the global inventory of Hg emissions for 2010 (AMAP/UNEP, 2013). Results of the 2015 anthropogenic emissions inventory are presented in detail in the Technical Background Report to the Global Mercury Assessment 2018 (AMAP/UNEP, 2019); with methods and underlying data extensively described in the technical annex to that report (available at https://www.amap.no/documents/doc/technical-background-report-for-the-global-mercury-assessment-2018/1815). The inventory estimates national emissions for ~220 countries in 11 subcontinental regions for each of the 17 main emission sectors. Tables 1 and 2 summarize, by region and source sector, the resulting 2015 emission estimates, which total ~2220 Mg of Hg (2000–2820 Mg).

The 2015 inventory estimates identify sources in Asia as responsible for about 50% of global Hg emissions in 2015, with East and Southeast Asia contributing ~40% and South Asia contributing ~10% (see Table 1). This reflects the growth in industrial development in these regions in recent decades and, in particular, the use of coal as a primary source of energy. Stationary combustion of fossil fuels and biomass burning is responsible for some 24% of estimated global Hg emissions (21% from coal burning). Industrial activities involving high-temperature processes, such as ferrous and non-ferrous metal smelting and cement production, are responsible for a further 28% of global Hg emissions.

The other main sources of Hg emissions are associated with the intentional use of Hg. These include use in mercury-added products, such as lamps, batteries, and instruments (e.g., medical instruments, such as thermometers, sphygmomanometers, and measuring devices, such as barometers) as well as in dental amalgam, all of which generate wastes that are sources of emissions, especially where these wastes are subject to uncontrolled burning. The intentional use of Hg also includes its use in industrial processes, such as the manufacture of vinyl chloride and the production of chlor-alkali using the mercury-cell process. However, by far the largest source of Hg emissions from intentional Hg use is that associated with ASGM, which globally is estimated to contribute ~38% of the total anthropogenic emissions inventory and ~68% of emissions in the Southern Hemisphere. The majority of ASGM emissions occur between 30°N and 30°S; ASGM contributes ~70% of emissions in South America and up to 80% of emissions in Sub-Saharan Africa as well as contributing a significant part of the emissions in East and Southeast Asia. As a result, South America and Sub-Saharan Africa are responsible for ~18% and ~16% of global emissions of Hg, respectively. However, if ASGM emissions are excluded, the pattern of regional contributions changes, and regions such as South Asia and CIS (Commonwealth of Independent States), and other European countries appear higher in the ranking. Overall, the patterns of both regional and sectoral contributions to global emissions in 2015 were similar to those in 2010.

The inventory methodology also recognizes that there may be additional emissions from sectors that it is not possible to quantify using the current methodology and available data; these could contribute between an additional few tens to several hundreds of Mg of Hg emissions per year. These include anthropogenic emissions associated with the incineration of industrial and sewage sludge and some hazardous wastes, oil and gas extraction (upstream of refineries), and agricultural burning. Some of these sources may be significant in a local and/or Arctic context.

Estimates of global Hg emissions from agricultural burning are included in the Emissions Database for Global Atmospheric Research (EDGAR; see Section 2.1.4), consistently increasing and almost doubling from 1970 to 2012 and totaling ~90 Mg in 2012 (Muntean et al., 2018). In 2012, their

Table 1
Contributions from various regions to the estimated global inventory of anthropogenic Hg emissions to air in 2015 for four main groups of emissions sectors (AMAP/UN Environment, 2019).

Region	Sector group (emissions, Mg)					
	Fuel combustion	Industry sectors	Intentional-use (including product waste)	Artisanal and small-scale gold mining	Regional total in Mg (range)	% of global total
Australia, New Zealand & Oceania	3.57	4.07	1.15	0.0	8.79 (6.93–13.7)	0.4
Central America and the Caribbean	5.69	19.1	6.71	14.3	45.8 (37.2–61.4)	2.1
CIS & other European countries	26.4	64.7	20.7	12.7	124 (105–170)	5.6
East and Southeast Asia	229	307	109	214	859 (685–1430)	38.6
EU28	46.5	22.0	8.64	0.0	77.2 (67.2–107)	3.5
Middle Eastern States	11.4	29.0	12.1	0.225	52.8 (40.7–93.8)	2.4
North Africa	1.36	12.6	6.89	0.0	20.9 (13.5–45.8)	0.9
North America	27.0	7.63	5.77	0.0	40.4 (33.8–59.6)	1.8
South America	8.25	47.3	13.5	340	409 (308–522)	18.4
South Asia	125	59.1	37.2	4.50	225 (190–296)	10.1
Sub-Saharan Africa	48.9	41.9	17.1	252	360 (276–445)	16.2
Global inventory	533	614	239	838	2220 (2000–2820)	100.0

share in the total global Hg emissions estimated by EDGAR was about 5%, with the greatest contributions to agricultural emissions from Brazil (17%), India (15%), and Indonesia (11%).

Comparing the 2015 global inventory results (AMAP/UNEP, 2019) with other national and regional emissions estimates is not straightforward. No comparable global inventories exist for 2015. However, Muntean et al. (2018) have compared global emissions estimates of Hg from the Emission Database for Global Atmospheric Research (EDGAR) in 2010 (totaling ~1770 Mg) with the 2010 GMA inventory estimates reported in AMAP/UNEP, 2013 (which updated totaled ~1810 Mg; AMAP/UNEP, 2019).

Comparisons between the 2015 AMAP/GMA inventory estimates and other national estimates from countries that maintain emissions inventory systems and with regional estimates for 2015 reported under the United Nations Economic Commission for Europe (UNECE) Convention on Long-Range Transboundary Air Pollution (CLRTAP) indicated a generally reasonable level of consistency with respect to estimates for national total emissions, considering the associated uncertainties (AMAP/UNEP, 2019). However, estimates for particular emissions sectors were more variable, reflecting a large degree of differences in the way emissions are classified or categorized under different Hg emissions reporting systems, many of which have been adapted from systems developed for reporting emissions of other pollutants. These major considerations would need to be addressed in any regulatory emissions reporting context.

2.1.2. Geospatial distribution and speciation of emissions

An important additional component of the work on the AMAP/GMA global mercury emission inventories involves their geospatial distribution to generate datasets that could then be used by modelers investigating, for example, long-range atmospheric transport of Hg (see Sections 4 and 5). As with the methods for preparing global emissions estimates, the methods used for spatial distribution have developed over time (Pacyna et al., 2003, 2010; Wilson et al., 2006; Steenhuisen and Wilson, 2015). For the 2015 inventory, this work comprised allocating national Hg emissions totals to specific point sources, or their area-wide distribution (within 0.25° grid cells) based on expected emissions distributions for the sectors concerned. The methods applied and the results of this work are detailed in Steenhuisen and Wilson (2019). Fig. 1 presents the geospatially distributed inventory for total mercury emissions (THg) viewed from an Arctic perspective.

At the same time as spatially distributing emissions, the approach employed in the GMA work also assigned emissions to three Hg species classes using a generic speciation scheme to classify total mercury (THg) emissions between GEM, GOM, and PBM according to the source sector concerned,

Table 2
Contributions from various source sectors to the estimated global inventory of anthropogenic Hg emissions to air in 2015 (AMAP/UN Environment, 2019).

Sector	Mercury emission (range), Mg	Sector % of total
Artisanal and small-scale gold mining (ASGM)	838 (675–1000)	37.7
Biomass burning (domestic, industrial and power plant)	51.9 (44.3–62.1)	2.33
Cement production (raw materials and fuel, excluding coal)	233 (117–782)	10.5
Cremation emissions	3.77 (3.51–4.02)	0.17
Chlor-alkali production (mercury process)	15.1 (12.2–18.3)	0.68
Non-ferrous metal production (primary Al, Cu, Pb, Zn)	228 (154–338)	10.3
Large-scale gold production	84.5 (72.3–97.4)	3.8
Mercury production	13.8 (7.9–19.7)	0.62
Oil refining	14.4 (11.5–17.2)	0.65
Pig iron and steel production (primary)	29.8 (19.1–76.0)	1.34
Stationary combustion of coal (domestic/residential, transportation)	55.8 (36.7–69.4)	2.51
Stationary combustion of gas (domestic/residential, transportation)	0.165 (0.13–0.22)	0.01
Stationary combustion of oil (domestic/residential, transportation)	2.70 (2.33–3.21)	0.12
Stationary combustion of coal (industrial)	126 (106–146)	5.67
Stationary combustion of gas (industrial)	0.123 (0.10–0.15)	0.01
Stationary combustion of oil (industrial)	1.40 (1.18–1.69)	0.06
Stationary combustion of coal (power plants)	292 (255–346)	13.1
Stationary combustion of gas (power plants)	0.349 (0.285–0.435)	0.02
Stationary combustion of oil (power plants)	2.45 (2.17–2.84)	0.11
Secondary steel production *	10.1 (7.65–18.1)	0.46
Vinyl-chloride monomer (mercury catalyst) *	58.2 (28.0–88.8)	2.6
Waste (other waste)	147 (120 – 223)	6.6
Waste incineration (controlled burning)	15.0 (8.9–32.3)	0.67
Total	2220 (2000–2820)	100

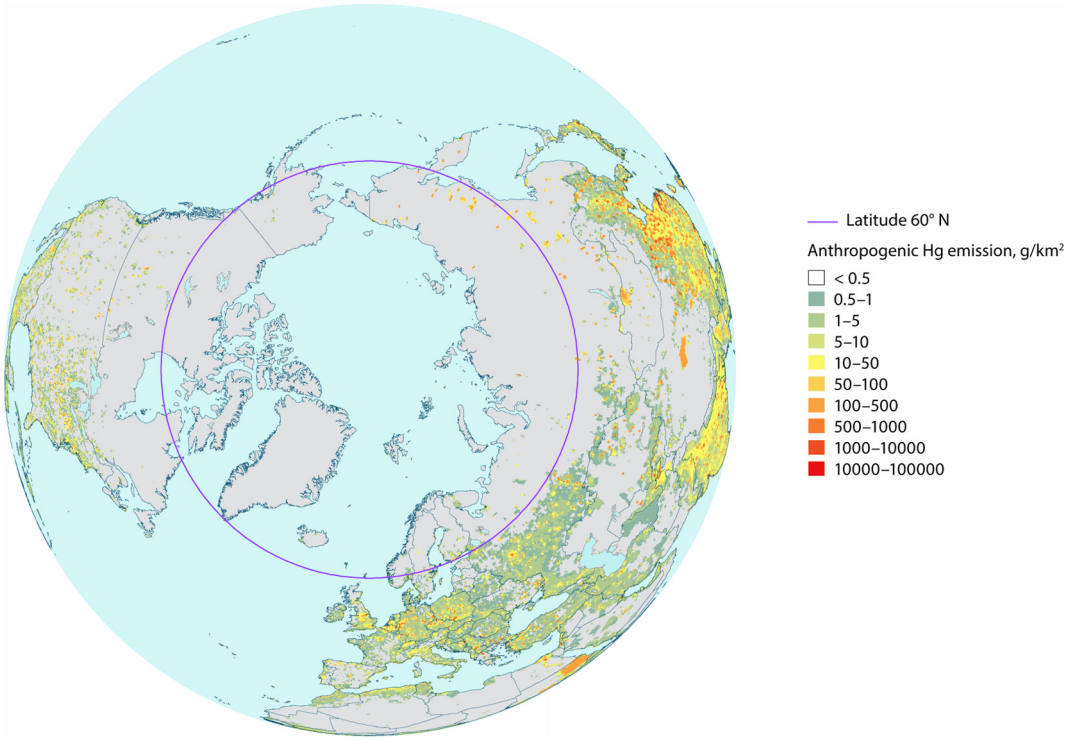

Fig. 1. Distribution of global anthropogenic mercury emissions showing proximity of emissions in major source regions to the Arctic.

and three emission height classes. An acknowledged deficiency in the GMA inventory work concerns the fact that the approach currently employed to define the Hg species that are emitted to the atmosphere is oversimplistic and outdated.

Mercury species emitted depend on several factors, including, inter alia, the air pollution control devices (APCDs) that are applied at emission point sources. The application of APCDs has changed considerably over recent decades, with developments taking place in different countries at different times. The use of combinations of APCD technologies, together with changing properties of fuels, raw materials and plant operating conditions, can have significant impacts on the mercury removal efficiency of APCDs (Zhang et al., 2016; Cao et al., 2022). The applied GMA inventory methodology incorporates the possibility to address such factors in quantifying emission totals, but this has not been reflected in GMA inventory geospatial distribution work to date—although the most recent inventory tools allow for this to be done, it was outside the scope of the work undertaken.

A large number of recent publications have documented speciation aspects of emissions, generally at large point sources such as power plants, smelters, and other industrial facilities, in particular in Asia (e.g., Wu et al., 2012; Zhang et al., 2015). This represents a considerable body of new information available to improve speciation schemes.

Muntean et al. (2018) performed a comprehensive literature review on Hg speciation for different sectors and developed three retrospective emissions scenarios based on different hypotheses related to the proportion of Hg species in the THg emissions. The reference scenarios use the split factors provided in AMAP/UNEP (2008), i.e. the scheme applied to all global anthropogenic Hg emissions inventories reported in AMAP and UN Environment GMA work (inventories for the years 1990–2015) as well as in EDGARv4.tox2. The other two scenarios apply split factors derived primarily from field measurements; from the United States Environmental Protection Agency's (EPA's) Information Collection Request (ICR; Bullock and Johnson, 2011), and scientific literature (Friedli et al., 2001, 2003a, 2003b; Park et al., 2008; Wu et al., 2012; Chen et al., 2013; Giang et al., 2015; Zhang et al., 2015), respectively. Fig. 2 presents the variation between the proportion of Hg(0) and reactive mercury (GOM and PBM) in the scenarios corresponding to the speciation scheme applied to the AMAP/GMA inventories and the scheme based on the reviewed scientific literature for different sectors. The share of the THg emissions that comprise Hg(II) species (gaseous and particulate) emissions was 25.3% for the reference scenario and 22.9% and 21.4% for the other two emissions scenarios. However, regional Hg speciation footprints may differ considerably depending on the characteristics of Hg-emitting sources located in different regions (see details in Muntean et al., 2018). Much of the recent literature on emissions speciation at industrial facilities concerns plants in East Asia (China, Japan, and the Republic of Korea), with speciation often dependent on the air pollution control technologies employed at the different plants. An evaluation of the three scenarios using the GEOS-Chem global 3-D Hg model showed a variation in deposition estimates of approximately ±10%. A comparison with measurements within a nested grid in sensitivity simulations for the United States indicated that speciated emissions estimated based on field measurements can improve wet deposition estimates near sources.

Changes in speciation from GEM to PBM or GOM would imply that Hg may be captured or deposited closer to its source regions and therefore have less potential for transport to the Arctic. Appropriate speciation of (geospatially distributed) Hg emissions datasets is important to modeling atmospheric transport from source to receptor regions including the Arctic (see Section 3). Steenhuisen and Wilson (2019) further investigated this for some major emissions sectors with respect to Chinese emissions using information compiled by Zhang et al. (2015). This clearly showed the influence of using updated speciation information, decreasing the relative proportions of GOM at locations associated with power plants and increasing the relative proportions of Hg(0) in areas of domestic and residential heating. Extending this work to the global scale would benefit from additional information on emissions speciation for other parts of the world. While newly available information on the speciation of emissions at major point sources presents the possibility for better addressing this aspect in future work; a significant knowledge gap still concerns the fate of Hg emitted from ASGM activities. Mercury used to amalgamate or concentrate gold is evaporated to recover the gold and is therefore by definition emitted as GEM. ASGM emissions occur close to the ground and thus the emitted Hg may be subject to faster removal via direct uptake by vegetation and by chemical

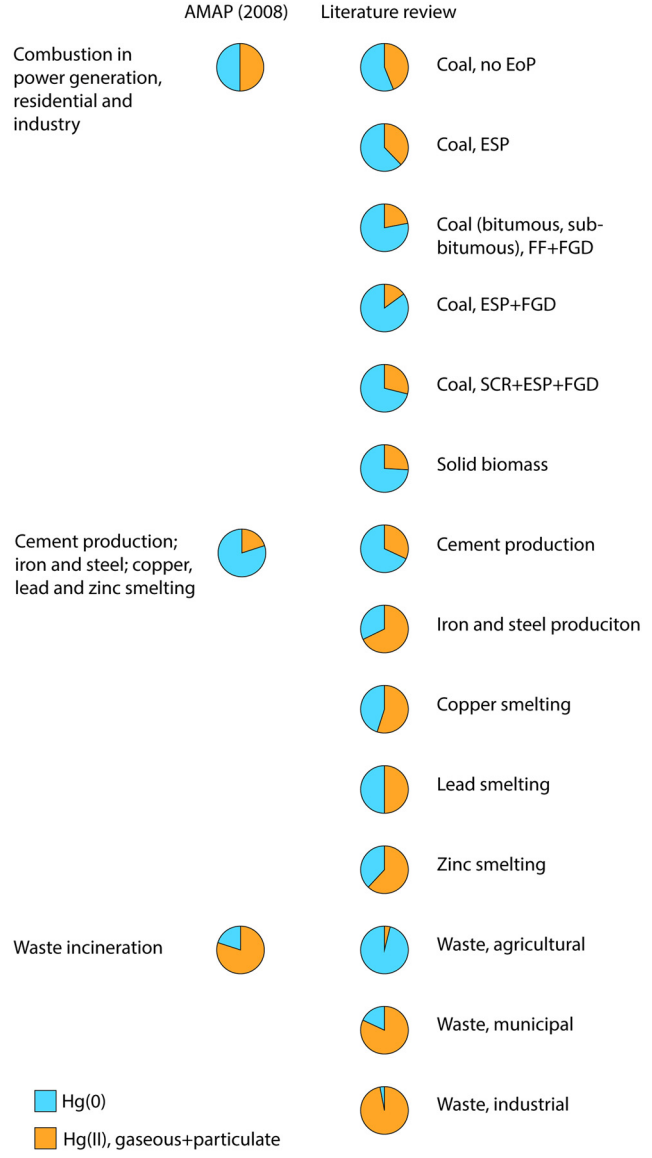

Fig. 2. Proportions of Hg(0) and Hg(II) (gaseous plus particulate) in the speciation scheme applied to the AMAP/GMA inventories for different sectors compared with information presented in recent literature (Muntean et al., 2018, and references cited therein). EoP: end-of-pipe measures; ESP: electrostatic precipitator; FF: fabric filter; FGD: flue gas desulfurization; SCR: selective catalytic reduction.

transformations through interaction with surfaces or adsorption to dust particles than might be the case for GEM emitted, for example, from power plant stacks (Gerson et al., 2022).

2.1.3. Anthropogenic emissions and releases in an Arctic context

The most recent AMAP assessment (AMAP, 2021) includes an updated Hg budget for the Arctic land and ocean (Dastoor et al., 2022), and the Arctic region is also evaluated in atmospheric transport source-receptor modeling work (see Section 5).

Based on the geospatial distribution of the 2015 emissions inventory, sources within the Arctic region (north of 60°N) contribute only a small part of global anthropogenic Hg emissions to air, ~14 Mg (<1%) of the total estimated inventory of 2220 Mg in 2015 (AMAP, 2021) (Table S1). It should be noted that this value has a relatively high associated uncertainty due to limitations of the spatial distribution methods for certain sectors in regions of sparse population. The majority of the anthropogenic Hg emissions in the Arctic region occur in Russia and are associated with relatively few point sources, including the non-ferrous metal smelters at Norilsk and on the Kola Peninsula (see Fig. 3). The Arctic also hosts coal-fired power plants along with other industrial facilities (including cement and ferrous metals production plants) in larger population centers, as well as mining and oil refining operations within or in close proximity to the Arctic. Smaller local emission sources are associated with diesel generators and waste dumps in smaller communities.

Although the anthropogenic Hg emissions within the Arctic region are small, it should be recognized that the Arctic States as a whole contribute significantly to global Hg emissions; these States together with other countries that are observers to the Arctic Council were responsible for ~44% of estimated global anthropogenic Hg emissions in 2015.

2.1.4. Trends in anthropogenic emissions

Mercury emissions to air have changed over time. Historically, gold and silver mining have been major sources of mercury emissions and releases. Following the industrial revolution and the subsequent rise of fossil fuel economies (i.e., from the 1850s onwards), Hg emissions increased (AMAP, 2011; AMAP/UNEP, 2019). Emissions during the first part of the 21st century are estimated globally at around 2000 to 2500 Mg yr^{-1} with emissions increasing in some geographical regions and decreasing in others.

Comparisons between global anthropogenic emission inventories produced at different times since the 1990s (AMAP, 1998, 2005, 2011; Pacyna and Pacyna, 2002; Pacyna et al., 2006, 2010) is complicated by the fact that, over time, additional sectors have been added to the inventories, as well as by changes in the methods applied for calculating emissions.

In the 2021 AMAP assessment (AMAP, 2021) it was only considered appropriate to compare the 2015 inventory results (AMAP/UNEP, 2019) with results from the 2010 inventory (AMAP/UNEP, 2013), as these were prepared using a similar methodology, and then only after the latter had been updated to introduce new sectors which were considered in 2015 (e.g., biomass burning in power generation, industry and domestic sources), newly available 2010 activity data, and some changes in methods for calculating emissions from ASGM and the disposal of Hg-added product wastes). The results (Fig. 4) indicate that estimated global anthropogenic emissions of Hg to the atmosphere for 2015 were approximately 20% higher than in 2010. Within this trend, modest decreases in emissions in North America and the European Union associated with continuing action to reduce emissions and shifts in fuels used for energy (i.e., away from coal) are more than offset by increased emissions in other regions, in Asia in particular. The overall trend appears to reflect a continuation of an upturn in global Hg emissions following decreasing emissions during the last decades of the 20th century, as described in the previous AMAP mercury assessment (AMAP, 2011), and also the possible impact of the global crisis of 2008 which depressed economic activity in the period of the 2010 inventory.

This contrasts somewhat with results of global Hg emissions estimates from EDGAR (Muntean et al., 2014, 2018) which show an increasing rather than a decreasing trend in global emissions in the last decades of the 20th century. Muntean et al. (2018) report global anthropogenic Hg emission trends over the period 1970 to 2012 based on an analysis of data from EDGAR (see Fig. 4). The EDGAR dataset applies a consistent methodology across all years. They show global emissions (excluding ASGM) increasing by 45% between 1970 and 2012.

In a recent review, Streets et al., (2019a), report annual trends in global emission in the period 2010–2015 applying a common menthodology. Their results, also shown in Fig. 4, are generally consistent with those produced under the GMA work for 2010 and 2015, but with higher overall total emissions in each of these years; by 22% and 8%, respectively.

Analysis of the magnitude of changes in estimated Hg emissions between 2010 and 2015 by region and sector in the GMA work (AMAP/UNEP, 2019) reveals that emissions in North America and the European Union (EU28) decreased across most sectors, resulting in modest decreases (~11 Mg) in total estimated emissions in each of these two regions (see Table S2). In all other regions, total regional Hg emissions increased between 2010 and 2015. In some regions, notably South America, increased

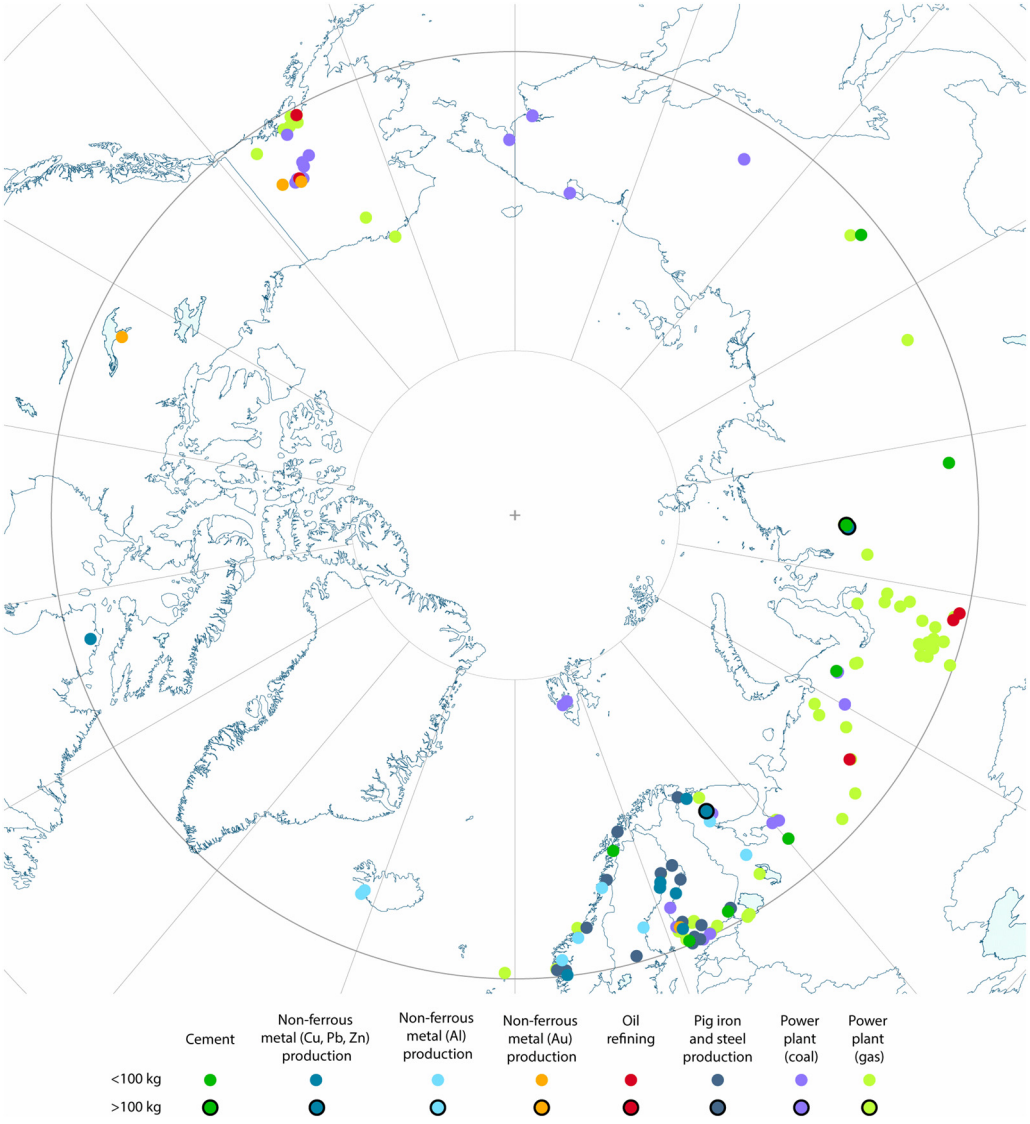

Fig. 3. Contributions and locations of anthropogenic point source mercury emissions in or close to the Arctic.

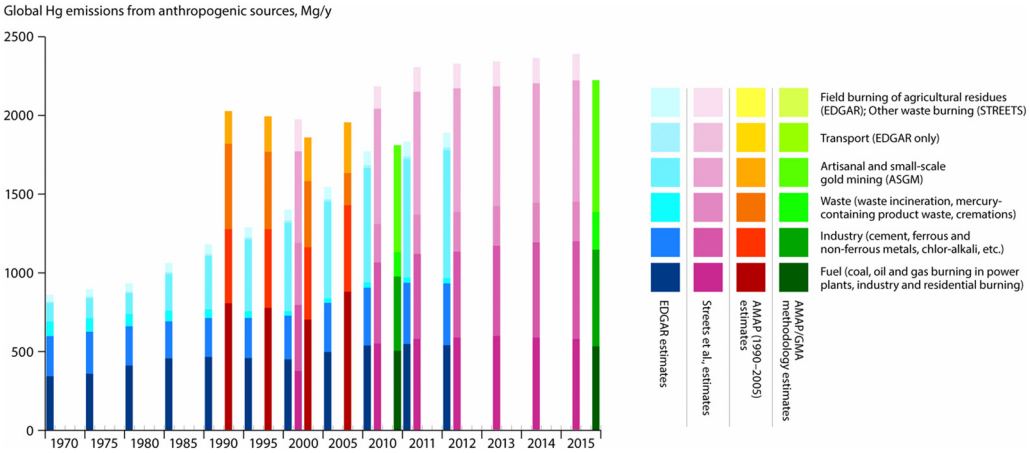

Fig. 4. Trends in global anthropogenic emissions of mercury to the atmosphere as produced by four emission inventory approaches. These approaches are not directly comparable as they use different methodologies, and do not necessarily include the same set of source sectors. AMAP/GMA estimates are reported in AMAP/UN Environment (2019); AMAP 1900–2005 estimates are from AMAP (2010); EDGAR estimates are from Muntean et al. (2014, 2018); Streets et al., estimates are from Streets et al. (2019).

ASGM activity contributed significantly to the increase in emissions both in percentage and absolute terms; in other regions, such as East and Southeast Asia, increased emissions are associated with industrial development and therefore are reflected in industry and energy sectors, in particular in non-ferrous metal production (NFMP). On a relative basis, the greatest increase was associated with Hg production in Central America and the Caribbean where Hg emissions grew by a factor of almost 20 due to new Hg production from mines in Mexico; industrial coal combustion also increased considerably in the same region (440%); however, in absolute terms, this corresponds to only a few Mg of emitted Hg. In absolute terms, the sectors showing the largest increases in estimated emissions of Hg were ASGM (159 Mg), NFMP (79 Mg), cement production (47 Mg), Hg-product waste disposal (32 Mg), and coal combustion in power plants (24 Mg), contributing to a total increase for all sectors of 413 Mg. Sectors with decreasing estimated emissions included (mercury-cell process) chlor-alkali production, which is being phased out globally, and oil combustion in the industry; however, the associated reductions were relatively small in absolute terms (6 Mg and 2 Mg, respectively). In general, apart from ASGM-related emissions, Hg emissions are strongly related to a growth in the industrial activity that in most regions reflects a growth in the consumption of fuels and raw materials to produce energy, cement, and ferrous and non-ferrous metals, among other activities. Increased industrial activity in many regions more than offsets emissions reductions achieved through, for example, more widespread application of air pollution control devices.

In addition to the challenges in comparing national/sector estimates over time, there are similar challenges with respect to comparing geospatially-distributed Hg emissions for different years/periods; here, there is the added complexity of documenting changes in the locations of emissions, particularly in the case of major point sources. Information concerning new power plants and industrial facilities, the closure of plants, and changes in fuels and technology applied at energy production and industrial facilities (e.g., to control emissions) is generally lacking or is not available in the public domain. This is a particular problem in areas with rapidly developing economies and in countries lacking consistent long-term tracking of Hg emissions.

The increasing trends in anthropogenic emissions in recent years are not generally reflected in Hg air concentrations observed at Arctic background air monitoring sites, most of which show decreasing trends, but increasing at a site in Western Canada where the trend has been attributed to increasing Asian emissions (MacSween et al., 2022). This inconsistency between emissions estimates and air concentration trends is likely related to the proximity of monitoring sites to regions where Hg emissions have declined significantly in recent decades (North America and Europe), to the effects of changes in speciation of emitted Hg, and to the influence of changes in re-mobilization, natural sources and deposition rates associated with climate change (see Section 4).

3. Modeling of atmospheric mercury transport to Arctic environments

This section briefly describes the atmospheric mercury transport, transformation, and removal mechanisms contributing to mercury in Arctic environments and its modeling.

3.1. Transport

In-situ measurements and modeling provide evidence for year-round transport of pollution from southern latitudes to the Arctic troposphere. Pollution transport to the Arctic is dominated by northern Eurasian sources in winter and by mid-latitude Asian and North American sources in spring (Sharma et al., 2013; Law et al., 2014; Monks et al., 2015; Willis et al., 2019). In spring, mid-latitude cyclones following a northerly course over eastern Asia and the North Pacific are frequent (Fuelberg et al., 2010). Evidence for springtime long-range transport events of atmospheric Hg from Asian sources to western North America and the Arctic is well documented (Jaffe et al., 2005; Weiss-Penzias et al., 2007; Obrist et al., 2008; Durnford et al., 2010; Moran et al., 2014). Durnford et al. (2010) analyzed Hg transport pathways to the Arctic and confirmed that Eurasian transport dominated in winter, while Asian and North American transport dominated in spring. The study estimated that the majority of long-range transport events in the Arctic originated in Asia (~55%) followed by events from Eurasian (~29%) and North American (~16%) sources.

The thermal stratification of the lower atmosphere at high latitudes, especially during the winter months, causes isolation of the High Arctic lower troposphere from lower latitudes creating a transport barrier referred to as the polar dome (Klonecki, 2003). The polar dome strongly influences the transport of air masses from mid-latitudes, increasing transport during winter and reducing during summer. The spatial extent of the polar dome strongly varies seasonally, from about 40° N polewards in the winter, when it envelopes snow-covered North America and Eurasia, to roughly north of the 70° N in the summer (Klonecki, 2003; Jiao and Flanner, 2016). This transport barrier is frequently disturbed by synoptic-scale weather systems that foster exchange between mid-latitude and Arctic air masses.

Recent measurement campaigns such as POLARCAT-IPY and NETCARE (Law et al., 2014; Bozem et al., 2019) provided evidence for three primary pollution transport mechanisms to the Arctic lower troposphere from major anthropogenic emission regions (Stohl, 2006): (1) low-level transport over snow-covered regions in winter, primarily from northern Eurasia; (2) low-level transport from mid-latitude regions located within the polar front (mainly in Europe) followed by uplift at the Arctic front and slow descent; and (3) upper tropospheric transport from southern mid-latitudes (mainly from North America) and Asia due to lifting of air mass by convention or warm conveyor belts and slow descent in the Arctic due to radiative cooling. In contrast to the low-level transport, oxidation and wet scavenging can remove a significant amount of Hg outside the Arctic in high-level transport. The lower troposphere in the Arctic is highly stably stratified during the winter months, with surface inversions persisting for several days; these conditions result in reduced dry deposition of pollutants during the transport process. Additionally, the lower troposphere is extremely dry in winter, which prevents precipitation scavenging. The age of the surface air in the High Arctic is about one week in winter and two weeks in summer and reduces to about 3 days in the upper troposphere (Stohl, 2006). In addition to the above pathways, transport of smoke plumes from boreal wildfires into the Arctic has been reported (Paris et al., 2009); Hg emitted during strong boreal wildfire events can be lofted by pyroconvection and entrained into the polar environment (Peterson et al., 2018).

Tropospheric transport in and around the Arctic is marked by a pronounced continental flow in winter and a zonal transport over the marine environment in summer. Synoptic-scale atmospheric transport to the Arctic from major emission source regions is primarily driven by three major semi-permanent pressure systems, most pronounced in winter. These include a low pressure system located in the sub-polar North Pacific Ocean just south of the Bering Sea (the Aleutian Low), a low pressure center southeast of Greenland near Iceland (the Icelandic Low), and a high pressure system situated over eastern Siberia (the Siberian High) (Bottenheim et al., 2004). Air circulation around the Icelandic Low, aided by the Siberian High, transports pollution from northern Europe and Siberia into the Arctic (AMAP, 2011). Pollutants from North America reach northern Europe along the southern portion of the Icelandic Low. The Aleutian Low induces an eastward flow of air along its southern portion from East Asia to northwestern Canada, Alaska, and into the western Arctic. The same air circulation transports pollutants from western North America into the Arctic. In the summertime, changes in land-sea contrast in surface heating lead to the weakening of low pressure systems and the replacement of continental highs by low pressure systems, causing a seasonal shift in air transport patterns. Durnford et al. (2010) and Octaviani et al. (2015) identified main export routes of pollution air masses from the Arctic through northeastern Canadian Arctic and eastern Siberia.

Mid-latitude atmospheric blocking events, characterized by a high-pressure center around 60°N and a low-pressure center to the south lasting up to 15 days, are known to significantly increase the transport of air pollution to the Arctic (Davini et al., 2012). Blocking events are more frequent in winter and spring, predominantly observed in the northeastern Atlantic

Ocean and to a lesser extent in the northeastern Pacific Ocean. The Arctic Oscillation (AO) and the North Atlantic Oscillation (NAO) are the two dominant sources of large-scale variability in northern hemisphere climate that affect pollution transport to the Arctic (Duncan and Bey, 2004; Hirdman et al., 2010). The AO is a hemispheric-scale mode of oscillation in atmospheric circulation, with large anomalies over the North Atlantic and North Pacific oceans. During a positive AO phase, surface pressure is abnormally low in the Arctic, which leads to efficient high mid-latitude pollutant transport from Western Europe and eastern North America to the Arctic (Feldstein, 2002; Eckhardt et al., 2003). The NAO is a regional pattern associated with the strength of Icelandic Low, and mainly influences the strength of the westerlies over the North Atlantic and Eurasia (Eckhardt et al., 2003). During the positive phase of the NAO, pollution transport from Europe is enhanced, particularly in winter and spring. Conversely, during the negative phase of the NAO (weaker Icelandic Low), air transport to the Arctic from Europe and Siberia is reduced, and from North America increased. Both oscillations (AO and NAO) exert the greatest influence on Arctic transport during winter and the weakest during fall.

The above atmospheric pathways can directly transport Hg-rich air masses from global anthropogenic Hg source regions to the Arctic. However, the long lifetime of Hg(0) in air and its global-scale transport and mixing result in a nearly well-mixed tropospheric background of Hg. Atmospheric transport of background Hg from lower latitudes accounts for the majority of Hg found in the Arctic environment. In addition, Hg transport to the Arctic is amplified as emitted Hg is successively deposited to surfaces and reemitted back into the air during its movement in the direction of the prevailing winds favoring higher Hg accumulation rate in the colder regions such as the Arctic. In the Arctic, mercury accumulates in vegetation, soils and glaciers at a rate comparable to or higher than in the lower latitudes (Dastoor et al., 2022). Cryptogamic vegetation such as lichen and mosses (dominant Arctic vegetation) have substantially higher Hg concentrations than vascular plants (mean: 62 ± 41 ng g^{-1} in lichen, 61 ± 39 ng g^{-1} in mosses, and 10 ± 5 ng g^{-1} in vascular plants), which leads to relatively high bulk vegetation Hg concentrations in the Arctic (mean: 49 ± 37 ng g^{-1}) (Dastoor et al., 2022). Overall the studies suggest that tundra ecosystems contain aboveground Hg biomass pools of up to 29 μg m^{-2} compared to boreal and lower-latitude forests with much longer growing seasons (15–45 μg m^{-2}) (Obrist et al., 2017; Olson et al., 2019; Wohlgemuth et al., 2020). Arctic soils have accumulated large pools of Hg (~597 Gg, 0–3 m depth) via atmospheric Hg deposition over millennia (Lim et al., 2020). Observations in Western Siberia show notably increasing accumulation of Hg in soils with latitude from 0.8 mg m^{-2} at 56°N to 13.7 mg m^{-2} at 67°N (0–1 m depth), suggesting substantially lower losses of soil Hg via re-emission in the higher latitudes (Lim et al., 2020).

Several mechanisms drive the inter-hemispheric pollution transport including vertical convective transport, seasonal changes in the Hadley circulation due to the shifting of the Intertropical Convergence Zone across the Equator, monsoon circulation as well as transport generated by eddies and wave breaking (Wu et al., 2018; Yan et al., 2021). Moreover, the inter-hemispheric transport is most efficient in the tropical region (between 30°N and 30°S) driven by convective lifting, where majority of the ASGM sources are located (~94% in 2015).

In recent decades, nearly twice the rate of rising in temperature in the Arctic compared to lower latitudes (Arctic amplification) is causing changes in the mid-latitude circulation patterns (Dobricic et al., 2016; Pithan et al., 2018). Warmer sea surface temperature and lower sea ice concentrations in the Arctic are linked to anomalies in wintertime atmospheric circulation (Lee et al., 2015; Francis et al., 2017), shown to impact pollution transport in the Arctic (Pozzoli et al., 2017; Chételat et al., 2022).

3.2. Transformation and removal

In addition to atmospheric transport, the oxidation of Hg(0) to Hg(II) strongly influences the dispersal of Hg in the atmosphere due to high deposition velocities of oxidized Hg (GOM and PBM) relative to Hg(0). Oxidation of Hg(0) reduces residence time for Hg in the atmosphere, and the reduction of Hg(II) to Hg(0) extends the residence time of Hg in the air. Knowledge of Hg redox chemical mechanisms and atmospheric concentrations of the key chemical reactants involved in Hg transformations are important to modeling Hg transformation and removal processes.

Laboratory experiments and investigations using theoretical chemistry have suggested rate constants for many gas-phase Hg oxidation processes. The reaction of Hg(0) with ozone has been studied in the laboratory (Pal and Ariya, 2004; Spicer et al., 2005; Rutter et al., 2012), but later it has been established that this reaction is not possible in the atmosphere since HgO is not stable in the gas phase (Peterson et al., 2007). Although the feasibility of the OH-initiated oxidation of Hg(0) was questioned since the reaction intermediate HgOH was found to be unstable (Goodsite et al., 2004), Dibble et al. (2020) found that this channel could be more significant. Other oxidation pathways were reviewed by Subir et al. (2011, 2012), which include such species as Cl_2, Br_2, H_2O_2, BrO, and ClO, but oxidation rates are believed to be unimportant due to low concentrations and small rate constants (Horowitz et al., 2017). Currently, the Br-initiated oxidation mechanism is thought to be the main oxidation pathway of atmospheric Hg(0) (Jiao and Dibble, 2015; Saiz-Lopez et al., 2020). However, there exists significant uncertainty in the concentrations of Br (Wang et al., 2019). The role of Hg(II) photo-reduction in the gas phase still needs to be further investigated and implemented into contemporary models (Saiz-Lopez et al., 2018; Saiz-Lopez et al., 2019). The Hg(II) partitioning bettwen gas (GOM) and condensed (PBM) phase is another factor determining the Hg atmospheric lifetime against dry and wet deposition (Amos et al., 2012; Steffen et al., 2014). Toyota et al. (2014) proposed that multiphase Br chemistry could play a role in the partitioning of Hg(II) between GOM and PBM. The mechanisms of gas-phase mercury redox chemistry are mostly known from computational studies, and more experimental studies are needed to confirm the rate constants. Additional studies are also needed to improve the understanding of oxidation and reduction reactions of Hg at environmental surfaces and aqueous environments.

The springtime photochemical release of gaseous Br to air from snow on sea ice and coastal land surfaces in the polar region and the rapid oxidation of ambient Hg(0) to Hg(II) via Br chemistry and subsequent deposition of Hg(II) to the surfaces lead to atmospheric mercury depletion events (AMDEs; Steffen et al., 2008). During these events, the gaseous Br concentrations increase to excessive levels not observed in other seasons of the polar atmosphere or other domains of the global atmosphere (Abbatt et al., 2012; Simpson et al., 2015). Oxidized Hg can either remain in the gas phase (GOM), adsorb to the surface of aerosol particles or be absorbed to aerosol bulk volumes (PBM; Lyman et al., 2020). Both forms of Hg (GOM and PBM) can either dry deposit directly to surfaces or be taken up by episodic precipitation and wet deposit in snowfall (Skov et al., 2006; Steffen et al., 2014). The deposition of Hg to surface snow is anomalously elevated during AMDEs (Wang et al., 2017). Deposited Hg(II) is primarily reduced to Hg(0) within snow due to photolytic-induced reactions. However, dark and biological reduction mechanisms in snow have been reported (Douglas et al., 2012). Using membrane-based methods, Osterwalder et al. (2021) measured 5 times higher atmospheric Hg(II) concentrations than measured by traditional denuder-based detection method at the Zeppelin Observatory on Svalbard (March–July 2019), and suggested that springtime atmospheric Hg(II) deposition has been underestimated in the Arctic marine environment.

High-latitude locations, particularly in the northern Arctic, experience two markedly different seasons, each with its own unique Hg deposition mechanisms. As in lower latitudes, Hg species can be deposited directly to vegetation surfaces (Demers et al., 2013; Jiskra et al., 2017; Obrist et al., 2017; Zhou et al., 2021), organic matter (Bartels-Rausch et al., 2011), and water during the summer and to snow/ice surfaces in winter by precipitation and dry deposition (Skov et al., 2006). In earth's high latitudes, where winter lasts for up to nine months, wintertime deposition of Hg to snow and ice surfaces can be significant. In the springtime, GOM produced during AMDEs is persistently scavenged from the air by snow and ice crystals as well as dry deposited to snowpacks leading to anomalously elevated Hg deposition to snow and ice surfaces along the coast and over the Arctic

Ocean (Brooks et al., 2006; Douglas et al., 2008; Douglas et al., 2012; Douglas and Blum, 2019). Once deposited to the snow pack, an average of 40–90% of Hg in the High Arctic snowpack is re-emitted to the atmosphere by photo-reduction prior to snowmelt (Ferrari et al., 2005; St. Louis et al., 2005; Johnson et al., 2008; Durnford et al., 2012; Durnford and Dastoor, 2011). However, in coastal and oceanic regions, a high percentage of snowpack Hg is retained and released in snowmelt (Douglas et al., 2012; Durnford et al., 2012; Dastoor and Durnford, 2014; Douglas and Blum, 2019). The dry and wet deposition rates of Hg species control the overall lifetime of Hg in the atmosphere.

3.3. Models and simulations

Four chemistry transport models were applied to simulate air concentration and deposition fluxes of Hg in the Arctic: DEHM (Christensen et al., 2004; Skov et al., 2020), GEM-MACH-Hg (Dastoor et al., 2008; Durnford et al., 2012; Kos et al., 2013; Dastoor and Durnford, 2014; Fraser et al., 2018; Zhou et al., 2021), GEOS-Chem (Holmes et al., 2010; Fisher et al., 2012), and GLEMOS (Travnikov and Ilyin, 2009). Detailed description and evaluation of the models against observations are available in (Angot et al., 2016; Travnikov et al., 2017; Dastoor et al., 2022). All the models simulate emissions, atmospheric transport, transformations, and deposition of three Hg forms – GEM, GOM, and PBM. They differ in spatial resolution, vertical coverage, and model formulation in terms of driving meteorological data. All the models simulate the redox chemistry of Hg species in the atmosphere but differ in the realization of particular chemical mechanisms.

In the polar regions, the largest differences among the models relate to parameterizations of the Br-initiated mechanism of Hg oxidation during the springtime atmospheric Hg depletion events (AMDEs) and air-surface Hg exchange including re-emission from snowpack and evasion from the sea surface (Dastoor et al., 2022). Increased oxidation of Hg(0) during AMDEs in the Arctic is parameterized either by temperature-dependent springtime enhancement of Br species (GEM-MACH-Hg, Toyota et al., 2014; GEOS-Chem, Holmes et al., 2010; GLEMOS, Travnikov et al., 2017) or by faster oxidation rates depending on solar radiation and air temperature (DEHM, Christensen et al., 2004). Air-snow exchange is simulated using solar radiation-dependent parameterization of Hg(0) re-emission from snowpack (GEOS-Chem, Fisher et al., 2012, GLEMOS, Travnikov and Ilyin, 2009) or dynamic multilayer algorithm of air/snowpack/meltwater exchange (GEM-MACH-Hg, Durnford et al., 2012). Besides, Hg evasion from the Arctic Ocean waters and sea ice during summer is implemented (GEM-MACH-Hg, Durnford et al., 2012; GEOS-Chem, Fisher et al., 2012) to explain the observed summertime maximum in Hg(0) concentrations (Steffen et al., 2005; Berg et al., 2013).

Despite significant improvements in model simulations of Hg cycling in the Arctic atmosphere and the Arctic Ocean, important gaps remain. The Br-initiated oxidation of Hg(0) is expected to be dominant in the global troposphere. However, simulated data on atmospheric concentrations of atomic Br are uncertain, since modeling of Br chemistry is challenging in general and is especially complicated in polar environments. Knowledge gaps exist in the quantification of the processes controlling Br chemistry, and model studies have simulated springtime Br chemistry in the polar boundary layer with various levels of complexity.

The geospatially distributed global Hg anthropogenic emissions for 2010 and 2015 were used in the model simulations (Section 2). Besides, the models estimate primary and secondary Hg emissions from terrestrial surfaces as a function of environmental conditions and soil Hg content (Selin et al., 2008; Durnford et al., 2012). Geogenic Hg emissions are distributed according to the locations of Hg deposits, and the revolatilization of legacy Hg from soils and vegetation is distributed based on patterns of historic Hg deposition fluxes.

All four models were used to perform simulations of Hg dispersion on a global scale for 2015 with appropriate multi-year model spin-up. Additional simulations were conducted for 2010 to estimate changes in Hg concentration and deposition between 2010 and 2015 using three models (DEHM, GEM-MACH-Hg, GEOS-Chem). A set of model sensitivity simulations were also conducted to analyze the influences of meteorological and emissions factors on the changes in Hg levels. Additionally, a number of model sensitivity simulations were carried out to determine source apportionment of Hg deposition to the Arctic using all four models. For this purpose, the modeling results from simulations with zeroed-out emissions from particular source regions were subtracted from the base run with the full emissions field. The final modeling results of the model ensemble are presented as the median of four models (DEHM, GEM-MACH-Hg, GEOS-Chem, GLEMOS) for Hg concentration and deposition in the Arctic and the source apportionment and of three models (DEHM, GEM-MACH-Hg, GEOS-Chem) for evaluation of changes between 2010 and 2015.

4. Changes in atmospheric mercury in the Arctic between 2010 and 2015

The main factors driving changes in atmospheric Hg levels are anthropogenic, wildfire and other legacy emissions, and atmospheric transport, redox, deposition, and evasion processes. Long-term anthropogenic mercury emission inventories indicate that worldwide air emissions of Hg peaked around the 1990s and then declined until ~2005–2010 before continuing to rise again (Zhang et al., 2015; Streets et al., 2019b; AMAP emissions inventory; see Section 2.1.4). The meteorological factors that are contributing to changes in atmospheric Hg in warming Arctic include air and water temperature, precipitation, sea ice cover, air pressure at sea level, aerosol loading and optical properties, and wind speeds and their patterns (IPCC, 2013; AMAP, 2017; Meredith et al., 2019; Serreze and Barry, 2011; Pistone et al., 2014; Screen and Simmonds, 2010). Production of reactive halogen species that oxidize Hg is favored under conditions of increased first-year sea ice and more open sea ice leads (Abbatt et al., 2012). Convective mixing over more prevalent open leads to increase Hg(0) concentrations in near-surface air that can be oxidized and deposited to surrounding snowpacks (Moore et al., 2014; Douglas et al., 2005). Conversely, reduced sea ice can result in a net increase in Hg evasion from water to air, through enhanced Hg reduction and open water surface area (Chen et al., 2015).

Atmospheric Hg trends in the Arctic have been estimated to be decreasing at a rate of 0.6% yr^{-1} from 1995 to 2007 (Cole and Steffen, 2010; Cole et al., 2013). Long term Hg observations at the High Arctic sites show seasonally variable and annually neutral (Ny-Ålesund, Svalbard) to decreasing air concentrations of Hg(0) ($\leq$ 1.0% yr^{-1}, Alert, Canada, and Villum Research Station, Greenland) (Cole et al., 2013; Skov et al., 2020). Whereas, increasing springtime Hg(II) concentrations have been observed at Alert (9–17% yr^{-1}; Cole et al., 2013). Consistent with measurements at Alert, a decreasing trend in surface air Hg(0) concentrations in the Canadian Arctic (~0.8% yr^{-1} from 1990 to 2005) was modeled by Dastoor et al. (2015). The authors suggested that the decline in air Hg(0) was driven equally by the reduction in anthropogenic emissions and increase in net deposition of Hg due to a reduction in snow cover and greater first-year sea ice. In a recent study, MacSween et al. (2022) found trends in annual mean total gaseous mercury at 8 of the 11 measurements sites (including high-, coastal- and sub-Arctic) for the available years (average about 10 years) to be negative. The largest annual negative trends were found at Villum and Amderma (Russia) ($\sim -2.8\%$ and -2.3% yr^{-1}), and the lowest negative trends were observed at Ny-Ålesund and Alert ($\sim -0.6\%$ and -1% yr^{-1}).

Fig. 5. Model ensemble simulated mercury annual average surface air gaseous elemental mercury (Hg(0)) concentrations (a), wet deposition (b), and total deposition (c) in 2015. Model ensemble simulated changes in atmospheric mercury surface air concentrations of Hg(0) (d, g, j), wet deposition (e, h, k), and total deposition (f, i, l) between 2010 and 2015 due to changes in meteorology (d, e, f), emissions (g, h, i), and both emissions and meteorology (j, k, l). Circles show observations in the same color scale. Air concentrations, and wet and total deposition observations are from ECCC-AMM (Cole et al., 2013), AMNet (Gay et al., 2013), EMEP (Tørseth et al., 2012) and Obrist et al. (2017).

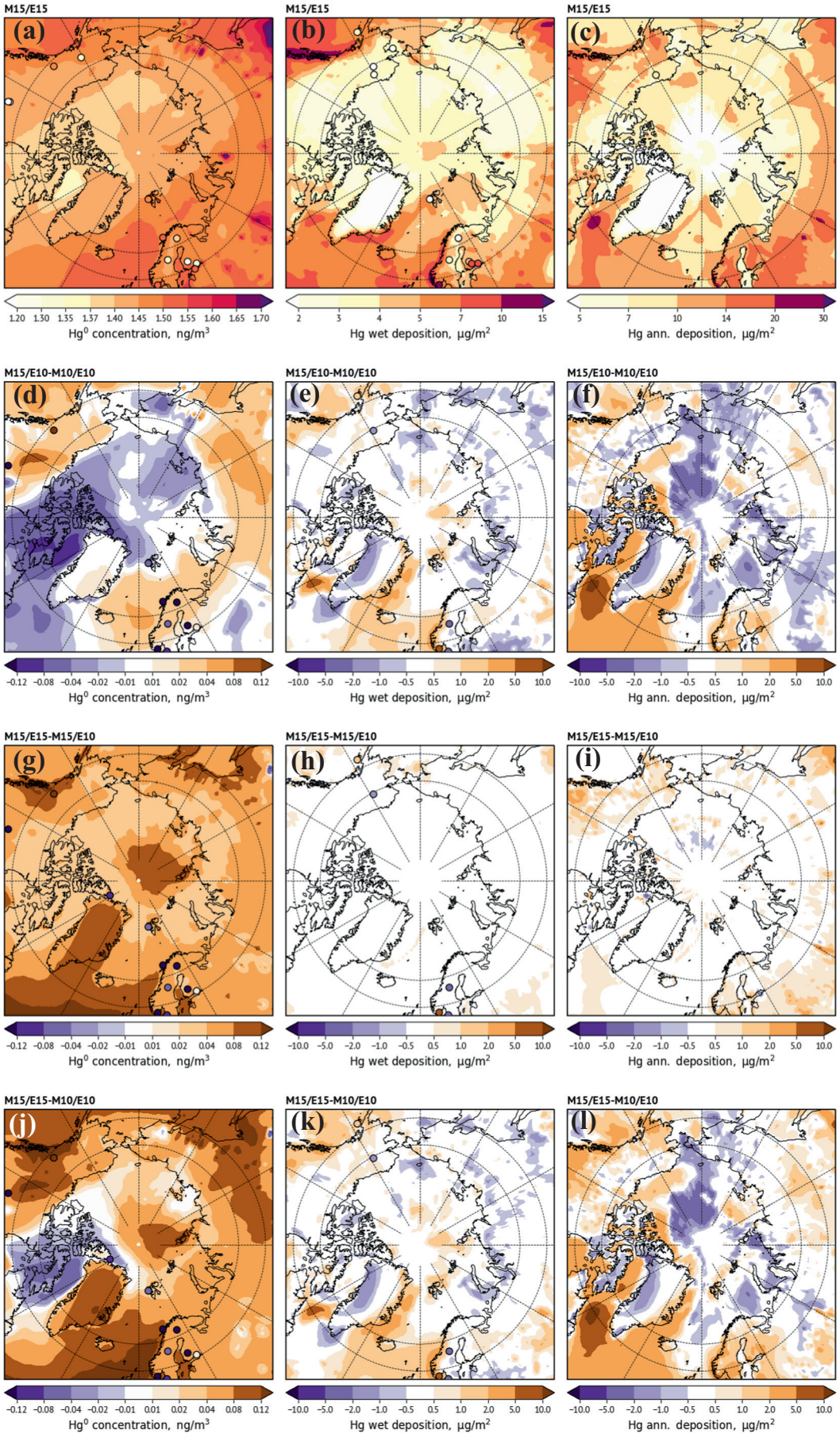
M15/E15
(a)
1.20 1.30 1.35 1.37 1.40 1.45 1.50 1.55 1.60 1.65 1.70
Hg⁰ concentration, ng/m³
M15/E15
(b)
2 3 4 5 7 10 15
Hg wet deposition, µg/m²
M15/E15
(c)
5 7 10 14 20 30
Hg ann. deposition, µg/m²
M15/E10-M10/E10
(d)
-0.12 -0.08 -0.04 -0.02 -0.01 0.01 0.02 0.04 0.08 0.12
Hg⁰ concentration, ng/m³
M15/E10-M10/E10
(e)
-10.0 -5.0 -2.0 -1.0 -0.5 0.5 1.0 2.0 5.0 10.0
Hg wet deposition, µg/m²
M15/E10-M10/E10
(f)
-10.0 -5.0 -2.0 -1.0 -0.5 0.5 1.0 2.0 5.0 10.0
Hg ann. deposition, µg/m²
M15/E15-M15/E10
(g)
-0.12 -0.08 -0.04 -0.02 -0.01 0.01 0.02 0.04 0.08 0.12
Hg⁰ concentration, ng/m³
M15/E15-M15/E10
(h)
-10.0 -5.0 -2.0 -1.0 -0.5 0.5 1.0 2.0 5.0 10.0
Hg wet deposition, µg/m²
M15/E15-M15/E10
(i)
-10.0 -5.0 -2.0 -1.0 -0.5 0.5 1.0 2.0 5.0 10.0
Hg ann. deposition, µg/m²
M15/E15-M10/E10
(j)
-0.12 -0.08 -0.04 -0.02 -0.01 0.01 0.02 0.04 0.08 0.12
Hg⁰ concentration, ng/m³
M15/E15-M10/E10
(k)
-10.0 -5.0 -2.0 -1.0 -0.5 0.5 1.0 2.0 5.0 10.0
Hg wet deposition, µg/m²
M15/E15-M10/E10
(l)
-10.0 -5.0 -2.0 -1.0 -0.5 0.5 1.0 2.0 5.0 10.0
Hg ann. deposition, µg/m²

In the Subarctic, Virolahti and Pallas (Europe) sites had no significant annual trends, but Little Fox Lake (Northwest Canada) had a significant increasing trend of $\sim +0.9\%\ yr^{-1}$. In addition, the High Arctic sites (Alert and Ny-Ålesund) revealed increasingly declining trend in recent years.

The model ensemble was applied to simulate atmospheric Hg transport and deposition to the Arctic in 2015 and their changes from 2010. The drivers for the changes in atmospheric Hg between 2010 and 2015 were analyzed. Fig. 5 presents simulated model ensemble Hg annual average surface air concentrations (Hg(0)), wet deposition, and total deposition in 2015, and their changes from 2010 due to changes in anthropogenic emissions and meteorology. The figures also compare modeled Hg levels and their changes with observations. The distribution of Hg in air and deposition in the Arctic and its evaluation were discussed in Angot et al. (2016) and Dastoor et al. (2022). Briefly, air Hg(0) concentrations are characterized by a latitudinal gradient with concentrations over 1.4 ng m^{-3} across most of the Subarctic and less than 1.4 ng m^{-3} over the Canadian Arctic Archipelago (CAA), Greenland, and the Arctic Ocean. While minimum Hg (0) concentrations driven by AMDEs are observed in spring (Steffen et al., 2008), maximum Hg(0) concentrations are observed in summer, which are attributed to Hg emissions from snow and sea ice melt and open ocean waters (Dastoor and Durnford, 2014) (see Fig. S1). The Arctic is characterized by low wet deposition fluxes (<5 μg $m^{-2}\ yr^{-1}$ vs. up to 30 μg $m^{-2}\ yr^{-1}$ in lower latitudes; Angot et al., 2016; Pearson et al., 2019; Gay et al., 2013), especially in the CAA, Greenland, and Siberia. Springtime wet deposition Hg fluxes can be anomalously high during AMDEs, primarily in coastal and marine regions (Steffen et al., 2013; see Fig. S2). Model ensemble simulated average total deposition fluxes of Hg are ~6.8 μg $m^{-2}\ yr^{-1}$ over land north of 60° N and ~ 7.4 μg $m^{-2}\ yr^{-1}$ over the Arctic Ocean. The highest modeled Hg deposition rates (up to 20 μg $m^{-2}\ yr^{-1}$) occur in the Subarctic where local Hg emissions (e.g., Europe), efficient trans-Pacific transport (northwestern North America), boreal forests, and relatively high precipitation rates (ocean around Greenland, and coastal northwestern Europe and North America) are found (Fig. 5c).

Model ensemble simulated changes in Arctic Hg air concentrations, wet deposition, and total deposition from 2010 to 2015 in response to meteorological conditions are shown in Fig. 5d-f. In general, changes in meteorology decreased the concentrations of Hg(0) in the CAA and the surrounding Arctic Ocean, Subarctic Canada (east), and the Baffin Bay, and increased concentrations in the rest of the Subarctic. Nearly opposite pattern is simulated in the changes of total deposition, indicating an influence of deposition processes on surface air concentrations of Hg(0). Model results suggest strongest increases in wet deposition over Southwest Alaska and Eastern Greenland to Scandinavia, driven by increasing precipitation in recent decades (see Fig. 6b) (Box et al., 2019; Mernild et al., 2015; Sprovieri et al., 2017), and to the Labrador sea due to enhanced Hg oxidation. The primary meteorology factors leading to the changes in atmospheric Hg are discussed later in the section. Changes in anthropogenic emissions (Fig. 5g-i) led to an increase in Hg(0) concentrations everywhere in the Arctic (most significantly in the Subarctic) between 2010 and 2015, driven by ~20% increase in global anthropogenic emissions (see Section 2). However, the impact of the increase in anthropogenic emissions is minor on wet and total deposition in the Arctic.

Overall changes simulated by the model ensemble in Arctic Hg air concentrations, wet deposition, and total deposition from 2010 to 2015 are shown in Fig. 5j-l. The simulations suggest a 0.01–0.10 ng m^{-3} increase in Hg(0) concentrations from 2010 to 2015 due to cumulative (meteorology plus emission) changes in most of the Arctic and 0.02–0.08 ng m^{-3} decrease in the CAA and surrounding ocean. These cumulative changes are relatively small, in agreement with observations, but more positive than observed in the Arctic (MacSween et al., 2022). The rise in emissions resulted in an increase in concentrations of Hg(0) at Little Fox Lake, in agreement with observations (MacSween et al., 2022). The simulated total annual Hg wet deposition flux in the Arctic was higher in 2015 than in 2010 by ~5 Mg yr^{-1}. The model ensemble annual Hg total deposition flux was higher in the Arctic (mainly due to increase in the Subarctic) by ~10 Mg yr^{-1} (with equal contributions from wet and dry depositions).

While there are differences between models, GEM-MACH-Hg simulations are used here to explain the influence of major meteorological factors that led to changes (between 2010 and 2015) in atmospheric Hg in the Arctic (Fig. 6). The changes in temperature and precipitation are shown in Fig. 6a-b. The impact of changes in air circulation characteristics on Hg transport to the Arctic was simulated for a Hg(0)-like passive tracer with 2015 anthropogenic Hg emissions and a fixed exponential decay corresponding to a lifetime of 6 months (Fig. 6c); no other Hg removal process was included. The NAO index was strongly negative in 2010 (NOAA, 2020). In contrast, 2015 was marked by a positive NAO phase. The NAO differences were most pronounced in winter and spring. The positive phase of the NAO is associated with below normal temperature and more sea ice in the Canadian Arctic (most pronounced in the east), Greenland, Baffin Bay, Davis Strait, and the Labrador Sea, and above normal temperatures across northern Europe often extending well into northcentral Siberia and the Arctic Ocean (Fig. 6a). The positive phase of the NAO is also associated with above-normal precipitation across the North Atlantic Ocean (between Greenland and Scandinavia) and northern Europe, predominantly in winter (Fig. 6b; Seager et al., 2020). During the negative phase of the NAO, opposite pressure, temperature, and precipitation anomalies occur.

Based on the past two decades of satellite measurements, Bougoudis et al. (2020) suggested that several factors such as air temperature, sea ice, atmospheric pressure, and winds play an important role in changes in tropospheric BrO concentrations over the Arctic. Bougoudis et al. (2020) found a moderate spatiotemporal relationship ($r = 0.32, p < 0.05$) between springtime tropospheric BrO concentrations and the first-year sea ice extent in the Arctic Ocean. Sea ice cover and thickness around the Villum Research Station have changed notably over the last decade (Selyuzhenok et al., 2020). Pöhler et al. (2010) measured BrO by active long-path differential optical absorption spectroscopy (LP-DOAS) and found that BrO concentrations were strongly correlated with temperature, increasing almost linearly with lower temperatures below −15 °C. A few more recent studies also established that lower temperatures promote BrO production in the Arctic (Swanson et al., 2020; Bognar et al., 2020; Seo et al., 2020).

Fig. 6d-l present GEM-MACH-Hg simulated atmospheric mercury surface air concentrations of Hg(0) and Hg(II), and evasion from the ocean waters and melting sea ice for the years 2010 and 2015 and their differences. The model simulations were conducted using meteorology for specific years while keeping anthropogenic Hg emissions fixed at the 2015 level. Satellite observations show significant BrO enhancements over coastal CAA, Baffin Bay, and north and east of Greenland in 2015 (Bougoudis et al., 2020). Higher BrO concentrations suggest the prevalence of enhanced bromine species involved in AMDE-led oxidation of Hg(0). Using field measurements, Stephens et al. (2012) examined the role of a large suite of halogen radicals in oxidizing Hg(0) in springtime, and suggested that Br and BrO are the dominant oxidants for Arctic AMDEs. Driven by increase in Hg(0) oxidation, the GEM-MACH-Hg model simulated significantly elevated concentrations of Hg(II) and lower concentrations of Hg (0) in these regions in 2015 relative to 2010 (Fig. 6d-i), which is in agreement with Hg(0) and Hg(II) observations at Alert and Ny-Ålesund (MacSween et al., 2022). Reduced oxidation of Hg over the Arctic Ocean north of Alaska and eastern Siberia in 2015 is also in-line with the decline in measured BrO concentrations over these regions. In addition, significantly lower sea surface temperature in the CAA and around Greenland in 2015 resulted in lower evasion fluxes of Hg(0) from melting sea ice and open waters, further reducing air concentrations of Hg(0) in these regions (Fig. 6j-l). Higher temperature over northern Europe in 2015 (compared to 2010) likely led to more vertical mixing of Hg(0) (deeper boundary layer height) in the source regions of Europe, and reduced surface air concentrations of Hg(0) (Fig. 6f). Octaviani et al. (2015) found that during positive phases of AO and NAO, net import of persistent organic pollutants to the Arctic tends to be lower than normal from North America, and higher from Asia (Urals − Siberia). While the Hg tracer-transport simulation suggests a similar impact on Hg transport to the Arctic (Fig. 6c), atmospheric Hg levels are found to be more sensitive to changes in temperature.

The general pattern of meteorological influence on atmospheric Hg suggested by the models is in-line with observations and is helpful in explaining observed trends. Meteorology-led changes combined with changes due to anthropogenic emissions resulted in an overall increase in modeled air concentrations of Hg(0) in the Arctic (predominantly in the Subarctic), in contrast with observed declines at most monitoring sites. It is likely that the impact of rising emissions is currently overestimated in the models, in tandem with underestimation of the influence of changes in meteorology. According to AMAP 2015 emission inventory (used in this study) global anthropogenic Hg emissions have risen between 2010 and 2015 by ~20%, primarily due to the rise in emissions from increased industrial activity in East and Southeast Asia and ASGM in South America. Whereas, the global anthropogenic emission estimates by Streets et al. (2019a) suggest a growth of 9.2% over the same time period. Anthropogenic emission speciation and release heights are uncertain (see Section 2.2.4; Zhang et al., 2015), and it is likely that shift in these parameters altered Hg redox and deposition processes that are not captured in the model simulations. Osterwalder et al. (2021) measured 5 times higher Hg(II) concentrations using membrane-based methods comapared to denuder-based detection method at the Zeppelin Observatory on Svalbard (March–July, 2019), suggesting significant underestimation of springtime Hg deposition in the Arctic marine environment. Recent observations in intact forests near intense ASGM activities in the Peruvian Amazon reveal exceptionally high total mercury concentrations in the atmosphere, canopy foliage, litterfall, and soils that are comparable to (or higher than) global industrial regions (Gerson et al., 2022). Majority of total Hg deposition (~94%) in the intact forests was driven by dry deposition of particulate and gaseous mercury to vegetation at a rate proportional to total leaf area, highlighting the role of the forest canopy in scavenging ASGM-derived Hg from the atmosphere. Model representations for Hg transformation and removal processes likely need revision to account for these observations.

Mercury models currently lack mechanistic representations of the activation of Br sources from snowpacks and blowing snow and the sea ice dynamics, important to the High Arctic Hg chemistry. The models did not account for the impacts of changes occurring in the terrestrial biosphere (such as the extent of vegetation cover and the length of the growing season, legacy and wildfire Hg emissions, and Hg emission from thawing permafrost) on air-surface Hg exchange processes. The biogeochemical changes in the terrestrial ecosystem are likely altering the legacy Hg fluxes (Chételat et al., 2022). Wildfire Hg emissions were estimated to be lower in 2015 compared to in 2010 (~2 Mg yr^{-1}; Dastoor et al., 2022), which is not taken into account in the model simulations. Vegetation Hg deposition is projected to increase with increasing vegetation cover and density (Wang et al., 2020). Conversely, Hg evasion from soils is projected to increase in response to permafrost thaw-led microbial reduction and release of stored Hg in soils (Schaefer et al. 2020). The development of fully interactive atmosphere-land-ocean biogeochemical models is needed to simulate the impacts of concurrent changes in biogeochemistry in the Arctic and global Hg emissions on Hg levels and explain Hg trends in the Arctic.

5. Source attribution of mercury deposition in the Arctic

The mercury model ensemble was applied to analyze detailed source apportionment of Hg deposition in various regions of the Arctic using AMAP global anthropogenic emissions of 2224 Mg yr^{-1} in 2015 (see Section 2), shown in Fig. 7–9. The model ensemble median annual Hg deposition (i.e., originating from contemporary global anthropogenic and geogenic emissions, and re-emission of legacy deposition) estimates north of 60° N and north of 66.5°N in the Arctic in 2015 are 243 ± 41 and 133 ± 31 Mg yr^{-1}, respectively. In the Arctic, contemporary global anthropogenic Hg emissions are responsible for 32% of annual Hg deposition (Fig. 7a), and seasonally for 35% in spring, 30% in winter, 28% in fall and 26% in summer. *Re*-emissions of legacy deposition (of anthropogenic and geogenic origin) from soils and oceans and primary geogenic emissions contribute to 64% and 4% of the annual Hg deposition in the Arctic, respectively (Fig. 7a). It should be noted that accumulated anthropogenic deposition in global ecosystems since the inception of industrial activities contributes to a larger portion of legacy re-emissions, which is expected to grow in the future in the absence of (or delayed) anthropogenic emission reduction efforts (Kwon and Selin, 2016). Seasonal contributions to annual anthropogenic Hg deposition in the Arctic (i.e., the portion of Hg deposition of contemporary anthropogenic origin) are distributed as 50% in spring followed by 25% in summer, 13% in fall and 12% in winter.

The models were applied to estimate the relative contributions of anthropogenic emissions of Hg from different sectors to the total annual anthropogenic Hg deposition in the Arctic (Fig. 7b). Total anthropogenic emissions of Hg were aggregated into four general groups: (i) power generation, 347 Mg yr^{-1} (15.6%), (ii) industrial sources, 874 Mg yr^{-1} (39.3%), (iii) intentional use and product waste, 166 Mg yr^{-1} (7.5%), and (iv) ASGM, 838 Mg yr^{-1} (37.6%; see Section 2.1.1). Chemical speciation of Hg emissions differs considerably between different sectors. Emissions from power generation consist of approximately equal contributions of elemental and oxidized forms of Hg. The proportion of oxidized Hg is much smaller in emissions from industrial sources (20%). One-fourth of the total Hg emissions from intentional use and product waste is emitted in the oxidized Hg forms. Whereas, all Hg emitted from ASGM is in elemental gaseous form. Due to the large proportion of oxidized Hg emissions from the power generation sector significant portion of Hg from this sector is deposited locally in the regions of major stationary combustion sources located in East and South Asia, Europe, North America, and South Africa. The power generation sector accounts for 17% of the total anthropogenic deposition of Hg in the Arctic. Hg emissions from the industrial sector are more widely distributed over the world and contain a substantial fraction of GEM (80%), resulting in approximately half (48%) of the anthropogenic deposition of Hg in the Arctic. The majority of ASGM emission sources are located in the low latitudes of both hemispheres; however, Hg emission from this sector, being in the elemental form, is transported globally and makes up 28% of the total anthropogenic deposition of Hg in the Arctic. The contribution from intentional use and product waste comes to 7%, which is consistent with the proportion of its share in total Hg emissions. It should be noted that speciation of Hg in emissions from different sectors is associated with significant uncertainties (see Section 2.1.2). Speciation of Hg emission influences the balance between long-range Hg transport and local Hg deposition and, in turn, the source attribution of anthropogenic Hg in the Arctic. Measured fractions of ~0.75 or higher of Hg(0) to total mercury in coal-fired power plant emission plumes have been reported in Europe, North America and China (Weigelt et al., 2016; Deeds et al., 2013; Wang et al., 2010). A recent global anthropogenic Hg emissions inventory (2010–2015) found that from 2010 to 2015 the fraction of Hg(0) to total Hg in worldwide emissions has remained stable at ~0.69, and Hg(0) fraction in coal combustion emissions slightly increased from ~0.61 to 0.63 (Streets et al., 2019a).

The proportions of annual anthropogenic Hg deposition from emissions in various global source regions to the Arctic are in the following order (Fig. 7c): East Asia (32%), CIS countries (12%), Africa (12%), Europe (8%), Southeast Asia (8%), South Asia (7%), South America (7%), Central America (6%), Arctic (3%), North America (3%), Middle East (2%), and Australia and New Zealand (0.1%). However, some seasonal differences exist, marked by distinct atmospheric circulations and deposition patterns (Fig. S1 & S2). The anthropogenic contributions from East Asia are 1.2, 1.5, 2.0, and 1.8 times higher than that of combined CIS and European contributions in winter, spring, summer, and fall, respectively. In summer and fall, the anthropogenic contribution from Africa dominates contributions from CIS countries and South Asian contribution dominates European contribution; the converse is the case in winter and spring.

The spatial distribution of the relative contributions of anthropogenic Hg deposition to the total annual Hg deposition simulated by the model ensemble in the Arctic is presented in Fig. 8a. The central and eastern High Arctic is estimated to receive a relatively higher proportion of annual Hg deposition from anthropogenic sources (30% to 50%) than the western High Arctic (≤30%). Anthropogenic deposition contributions of Hg are

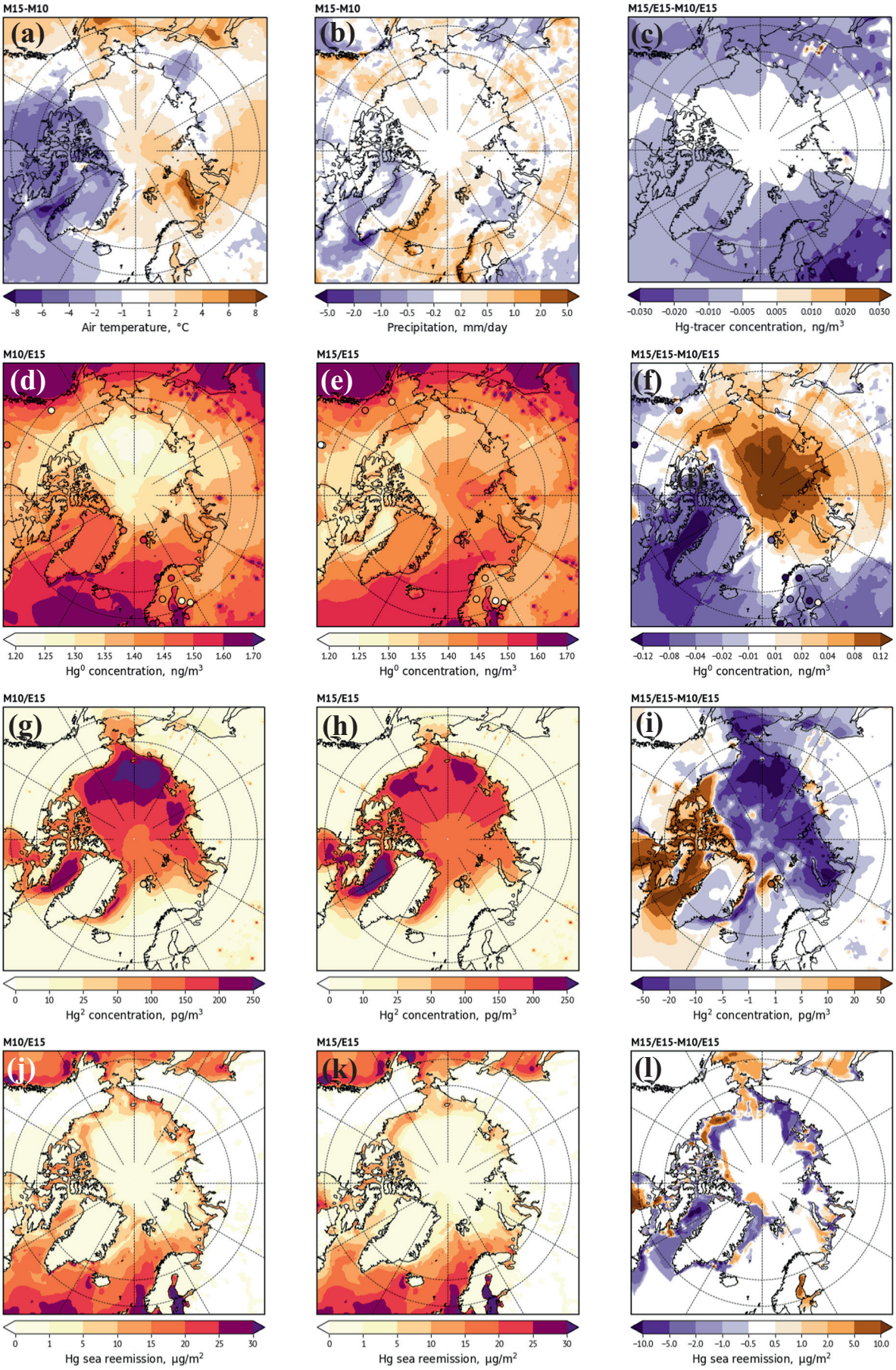
M15-M10
(a)
−8 −6 −4 −2 −1 1 2 4 6 8
Air temperature, °C
M15-M10
(b)
−5.0 −2.0 −1.0 −0.5 −0.2 0.2 0.5 1.0 2.0 5.0
Precipitation, mm/day
M15/E15-M10/E15
(c)
−0.030 −0.020 −0.010 −0.005 0.005 0.010 0.020 0.030
Hg-tracer concentration, ng/m3
M10/E15
(d)
1.20 1.25 1.30 1.35 1.40 1.45 1.50 1.60 1.70
Hg0 concentration, ng/m3
M15/E15
(e)
1.20 1.25 1.30 1.35 1.40 1.45 1.50 1.60 1.70
Hg0 concentration, ng/m3
M15/E15-M10/E15
(f)
−0.12 −0.08 −0.04 −0.02 −0.01 0.01 0.02 0.04 0.08 0.12
Hg0 concentration, ng/m3
M10/E15
(g)
0 10 25 50 100 150 200 250
Hg2 concentration, pg/m3
M15/E15
(h)
0 10 25 50 100 150 200 250
Hg2 concentration, pg/m3
M15/E15-M10/E15
(i)
−50 −20 −10 −5 −1 1 5 10 20 50
Hg2 concentration, pg/m3
M10/E15
(j)
0 1 5 10 15 20 25 30
Hg sea reemission, µg/m2
M15/E15
(k)
0 1 5 10 15 20 25 30
Hg sea reemission, µg/m2
M15/E15-M10/E15
(l)
−10.0 −5.0 −2.0 −1.0 −0.5 0.5 1.0 2.0 5.0 10.0
Hg sea reemission, µg/m2

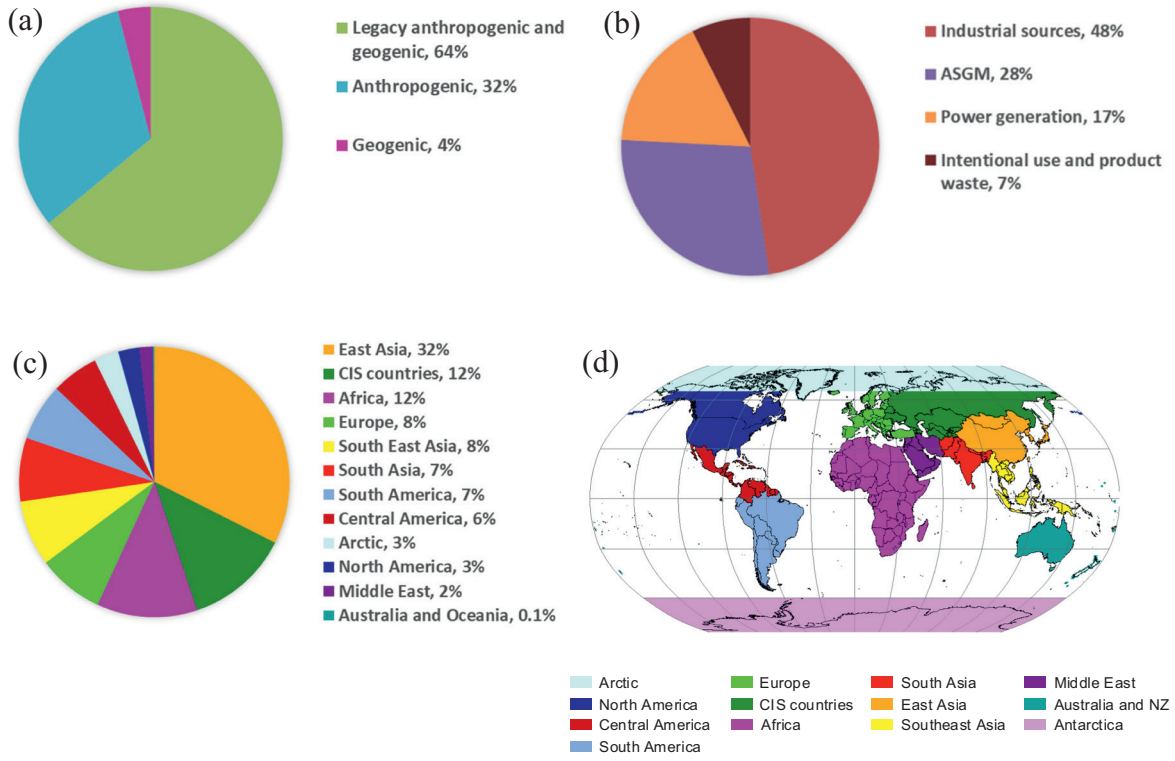

Fig. 7. Model ensemble simulated relative contributions of global anthropogenic, legacy (reemission of historic anthropogenic and geogenic deposition) and geogenic Hg emissions to annual total deposition of Hg (a) in the Arctic in 2015. Model ensemble simulated relative contributions of anthropogenic emissions from different sectors (b) and different source regions (c) to annual anthropogenic Hg deposition in the Arctic in 2015, and definition of global anthropogenic emission source regions (d).

lower to terrestrial surfaces (below 30%) than they are to the ocean with an exception of watersheds of the Yenisei and Kolyma rivers in Eurasia. The lowest anthropogenic contributions are estimated for the Mackenzie, Yukon, and Lena river basins, but these watersheds accumulate a relatively higher percentage of Hg deposition from wildfires (Fig. 9a). Measurements and model ensemble estimates suggest Hg runoff from Yenisey and Lena rivers to the Arctic Ocean to be the largest (Zolkos et al., 2020; Dastoor et al., 2022). In order to further analyze the spatiotemporal variations of global anthropogenic Hg emission contributions within the Arctic, seasonally distributed median anthropogenic Hg deposition contributions were estimated in six Subarctic regions (defined as 1–6 L) and six High Arctic regions (defined as 1–6H) using the model ensemble simulations (see definitions in Fig. 8a) (Fig. 8b-f). Subarctic regions mostly encompass terrestrial regions and the High Arctic regions cover oceanic surfaces, with an exception of the regions defined as 5 L and 5H (eastern Canada to western Greenland).

Average total Hg deposition fluxes from all emission sources in the Arctic range from 7.6 to 10.7 $\mu g\ m^{-2}\ yr^{-1}$ in Subarctic regions (10.7, 9.5, 8.6, 7.6, 10.4 and 8.6 $\mu g\ m^{-2}\ yr^{-1}$ in 1L, 2L, 3L, 4L, 5L, and 6L, respectively), and 3.6 to 8.9 $\mu g\ m^{-2}\ yr^{-1}$ in High Arctic regions (8.1, 7.7, 8.9, 6.3, 3.6 and 5.9 $\mu g\ m^{-2}\ yr^{-1}$ in 1H, 2H, 3H, 4H, 5H, and 6H, respectively). Generally, differences in anthropogenic Hg deposition contributions from emissions in various worldwide geographic regions to different Arctic regions (1–6L and 1–6H) are found to be small (Fig. 8b-f), reflecting a long lifetime of Hg in the atmosphere giving rise to a well-mixed distribution. The largest total anthropogenic contributions occur in 1L (3.33 $\mu g\ m^{-2}\ yr^{-1}$) and 5L (3.13 $\mu g\ m^{-2}\ yr^{-1}$), primarily reflecting proximity to mid-latitude anthropogenic sources and higher precipitation rates in these regions. Although total anthropogenic deposition contributions are comparable in 1L and 5L, the European contribution is twice that of the North American contribution in 1L, but comparable to the North American contribution in 5L. In the High Arctic, eastern regions (1–3H) receive larger total anthropogenic deposition contributions (2.6–2.9 $\mu g\ m^{-2}\ yr^{-1}$) than the western regions (1.1–1.9 $\mu g\ m^{-2}\ yr^{-1}$, 4–6H). The western High Arctic regions are characterized by both lower precipitation and lower import of emissions to the Arctic.

Seasonally, there are notable spatial variations in total anthropogenic Hg deposition contributions (Fig. 8c-f), mainly arising from inter-seasonal shifts in atmospheric circulation, precipitation, and vegetation regimes. In fall and winter, there is no clear distinction in contributions between Subarctic and High Arctic regions; the highest anthropogenic depositions in the Subarctic occur in 5L and 6L. Springtime anthropogenic contributions are exacerbated by AMDEs over sea ice, meaning that deposition is highest in High Arctic regions, especially in 1–3H. In summer, the northward retreat of the polar front limits the pollution transport to the High Arctic; additionally, efficient vegetation Hg uptake in temperate and Subarctic regions enhances anthropogenic Hg deposition in the Subarctic regions and lessens in High Arctic regions (see Fig. S2). Overall, relative contributions of anthropogenic Hg to the total Hg deposition are found to be slightly higher in High Arctic regions compared to Subarctic regions, and anthropogenic contributions are estimated to be highest in winter and spring (31% to 38%) and lowest in summer (25% to 28%).

Fig. 6. GEM-MACH-Hg simulated changes between 2015 and 2010 in air temperature in the springtime (a), yearly average precipitation (b), and surface air concentrations of mercury-like passive tracer (c). Hg(0) passive tracer simulation was conducted using 2015 anthropogenic Hg emissions, a fixed exponential decay corresponding to lifetime of 6 months and no other removal processes, and shows the impact of changes in meteorology on air transport characteristics. GEM-MACH-Hg simulated impacts of changes in meteorology: atmospheric mercury surface air concentrations of Hg(0) in 2010 (d), and 2015 (e), and their differences (f); surface air concentrations of Hg(II) in 2010 (g), and 2015 (h), and their differences (i); and Hg evasion from ocean waters and melting sea ice in 2010 (j), and 2015 (k), and their differences (l). The model simulations for the impact of changes in meteorology were conducted using meteorology for the specific years and anthropogenic Hg emissions fixed at 2015 level. Circles show observations in the same color scale.

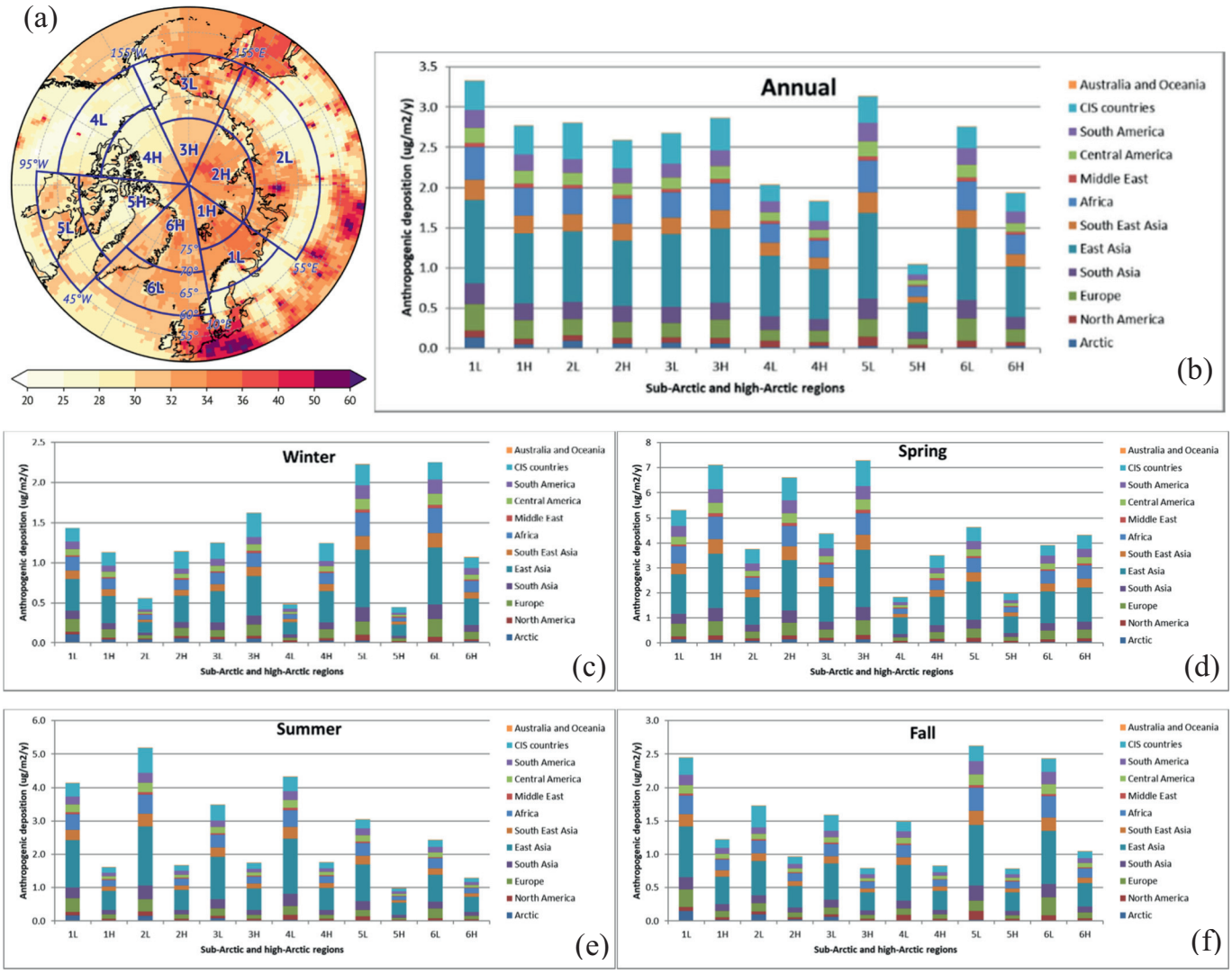

Fig. 8. Model ensemble simulated relative contributions of global anthropogenic Hg emissions to annual total deposition of Hg, and definitions of sub-arctic (1L-6L) and high-arctic (1H—6H) regions (a). Model ensemble simulated contributions of global anthropogenic Hg emissions from different source regions (bar colors) to total deposition Hg fluxes (μg/m^2/y) in sub-arctic and high-arctic regions in 2015: annual (b), winter (Dec.–Feb.) (c), spring (March–May) (d), summer (June-Aug.) (e), and fall (Sept.–Nov.) (f).

Measurements and modeling confirm that Hg deposition to vegetation, and thus summertime deposition, dominates other terrestrial deposition pathways and is a major source of Hg to boreal forests and tundra soils (Dastoor et al., 2022). Legacy Hg deposition accumulated in vegetation and active soils is released back to the atmosphere during wildfires (Friedli et al., 2001; Obrist et al., 2017; Fraser et al., 2018). Present-day global and Arctic (north of 60°N) wildfire emissions are estimated at 400–675 Mg yr^{-1} and ~20–200 Mg, respectively (see Section 2). Dominant source regions of wildfire emissions are Africa (43.8% of global emissions), Eurasia (31%), and South America (16.6%), and global wildfire Hg emissions are estimated to increase by 14% in 2050 due to climate change (Kumar and Wu, 2019). Models estimate that global wildfire emissions are responsible for 12–17 Mg yr^{-1} of Hg deposition in the Arctic, representing 6% to10% of annual Hg deposition in the Arctic (Kumar and Wu, 2019; GEOS-Chem simulation: Fig. 9a). Using GEOS-Chem, Kumar and Wu (2019) estimated wildfire contributions to the annual Hg deposition from Eurasia, Africa, and North America of 5.3%, 2.5%, and 1% in the Arctic spread across all seasons, but more than 50% of wildfire-induced Hg deposition originated from Eurasia and North America boreal forest fires in summer and fall. Fraser et al. (2018) reported that the western Canadian Arctic (the Northwest Territories and Yukon) is consistently more impacted by wildfires and found the Great Slave Lake region in the Northwest Territories to be a wildfire Hg deposition "hotspot". Recent measurements from lake sediment collected north of Great Slave Lake reported that charcoal deposition from wildfires since the late 1800s co-occurred with excess deposition of Hg to the lakes (Pelletier et al., 2020). GEOS-Chem simulation in Fig. 9a shows a highly variable spatial distribution of the impact of wildfire emissions in 2015 with wildfire contributions of over 20% in the Sub-arctic regions of western Canada and eastern Siberia. The proportion of Hg released as Hg(0) in wildfires varies between 50% and 95% based on aircraft measurements (Friedli et al., 2003b), satellite measurements (Finley et al., 2009), and laboratory experiments (Obrist et al., 2008; Kohlenberg et al., 2018), but models currently assume wildfire Hg mostly emitted as Hg(0) due to a lack of speciated wildfire emission inventories.

Finally, the model ensemble was applied to estimate the relative contribution of Arctic region emissions (emissions located north of 66°N) from human activities to total anthropogenic Hg deposition in the Arctic. Sources within the Arctic region contribute <1% (~14 Mg yr^{-1}) of the total estimated anthropogenic emissions of 2220 Mg yr^{-1} in 2015, the majority of which are located in Russia (see Section 2.1.3). The model ensemble estimates an average contribution of 3% from anthropogenic emissions in the Arctic region to the annual total anthropogenic Hg deposition in the Arctic (Fig. 7c), which is comparable to the contribution from North American anthropogenic sources. The spatial distribution of the relative impact of Arctic

region anthropogenic emissions on total anthropogenic Hg deposition in the Arctic is shown in Fig. 9b-f. Model ensemble results suggest that the relative contribution of Arctic region anthropogenic emissions to annual anthropogenic Hg deposition varies between 2% and 7% over the Arctic Ocean (Fig. 9b). On land, local anthropogenic sources account for up to 35% of anthropogenic Hg deposition in Eurasia annually. Anthropogenic emissions include a fraction of Hg emission as oxidized Hg, which contributes to high deposition to local landscapes owing to its short lifetime. Model results show that local anthropogenic sources influence the Hg deposition in Eurasian watersheds (e.g., the Yenisey and Kolyma watersheds), thus also contribute to river Hg runoff to the Arctic Ocean. It should be noted that there are additional anthropogenic Hg sources between 60 and 66°N that are not considered here. Fig. 9c-f present the seasonal differences in anthropogenic emission contributions from the Arctic region to seasonal total anthropogenic Hg depositions in the Arctic. Notable seasonal differences in Hg deposition contributions of local anthropogenic origin are found, driven by distinct seasonal atmospheric transport and deposition pathways (see Section 3). In winter and fall, efficient low-level Hg transport of north Eurasian emissions over frozen surfaces combined with inefficient removal processes lead to relative local anthropogenic contributions of 3% to 15% and over 15% to the eastern Arctic Ocean and High Arctic terrestrial regions, respectively. Conversely, in summer and spring, both weak transport into the Arctic polar dome and efficient wet and dry removal of Hg result in more deposition in the vicinity of sources on land and generally <3% contribution of local anthropogenic sources to the ocean.

6. Conclusions and recommendations

Estimated global anthropogenic emissions of Hg to the atmosphere for 2015 were 2220 Mg (range: 2000–2820 Mg), approximately 20% higher than comparable estimates for emissions to air in 2010. Most anthropogenic emissions of Hg occurred outside the Arctic, with only an estimated 14 Mg (0.63%) emitted north of 60°N. Mercury models support the conclusion that anthropogenic and legacy Hg emissions in other parts of the world are important sources of Hg to the Arctic, which is transported there via the atmosphere and ocean currents. Wildfires around the globe are an important re-emission pathway of legacy Hg to the atmosphere, including fires in the boreal forest in the Arctic (north of 60°N).

The model ensemble was applied to simulate the changes in atmospheric Hg transport and deposition to the Arctic between 2010 and 2015 and their drivers. The general pattern of meteorological influence on Arctic atmospheric Hg simulated by the models is in-line with observations and is helpful in explaining observed changes. The modeling results in combination with trends in observed atmospheric Hg and anthropogenic emissions reveal that changes in meteorology are having a profound impact on contemporary Hg cycling due to alterations in Arctic Hg physicochemical processes. In 2015, below normal temperature and more sea ice in the Canadian Arctic, Greenland and the surrounding ocean linked to the positive phase of NAO led to enhanced production of bromine species in these regions in spring and summer. Consequently, AMDE-led oxidation of Hg(0) was elevated in the Canadian Arctic Archipelago, eastern Subarctic Canada, northern Greenland, and surrounding ocean in 2015, which resulted in modeled increased air concentrations of Hg(II) and reduced air concentrations of Hg(0) in agreement with observations at Alert and Ny-Ålesund. Lower evasion flux of Hg(0) from melting sea ice and open waters driven by reduced sea surface temperature in 2015 further reduced air concentrations of Hg(0) in these regions. Model results estimated an overall increase in total deposition of Hg in the Arctic (~10 Mg yr^{-1}, equally from dry and wet depositions) in 2015 relative to 2010, mainly driven by Hg oxidation over waters in Canada, the Labrador Sea, and the Baffin Bay, and increase in precipitation from eastern Greenland to Scandinavia and in northwestern North America. The model results suggest that changes in meteorology can exacerbate the impact of global anthropogenic emissions on Hg deposition in the Arctic, especially in the regions more susceptible to climate warming.

When meteorology-led changes are combined with the recent increase in anthropogenic emissions, the model ensemble estimated an overall increase in surface air concentrations of Hg(0) in the Arctic from 2010 to 2015 (predominantly in the Subarctic), in contrast with observed declines at most monitoring sites (MacSween et al., 2022). It is likely that the impact of rising emissions is currently overestimated in the models, in tandem with underestimation of the influence of changes in meteorology. While global anthropogenic Hg emissions are estiamted to have risen by ~20% between 2010 and 2015 in the AMAP emission inventory, the emission inventory by Streets et al. (2019a) suggests a growth of 9.2% over the same time period. Anthropogenic emission speciation and release height are uncertain (Zhang et al., 2015), and shift in these parameters likely altered Hg redox and deposition processes that are not captured in the model simulations. The models did not account for the impacts of changes occurring in the terrestrial biosphere (such as the extent of vegetation cover and the length of the growing season, legacy and wildfire Hg emissions, and Hg emission from thawing permafrost) on air-surface Hg exchange processes (Chételat et al., 2022). Wildfire Hg emissions were estimated to be lower in 2015 compared to in 2010 (~2 Mg yr^{-1}; Dastoor et al., 2022), which was not taken into account in the model simulations. Osterwalder et al. (2021) measured 5 times higher atmospheric Hg(II) concentrations using membrane-based method than measured by traditional denuder-based detection method at the Zeppelin Observatory on Svalbard (March–July 2019), which suggests that springtime Hg deposition is currently underestimated in the Arctic marine environment. Observations in the Peruvian Amazon near intense ASGM activities reveal exceptionally high Hg concentrations in canopy foliage, litterfall, and soils, suggested to be driven by dry deposition of particulate and gaseous mercury to vegetation at a rate proportional to total leaf area (Gerson et al., 2022). Model representations for Hg removal processes likely need revision to account for these observations.

The model ensemble estimated that contemporary global anthropogenic Hg emissions (i.e., 2015) are responsible for 32% of the annual Hg deposition in the Arctic, re-emissions of legacy deposition (anthropogenic and geogenic origin) from soils and oceans for 64%, and primary geogenic emissions for 4%. Half of annual anthropogenic Hg deposition in the Arctic occurs in spring followed by 25% in summer, 13% in fall, and 12% in winter. Anthropogenic contributions to the total deposition of Hg in the Arctic were found to be highest in winter and spring (31% to 38%) and lowest in summer (25% to 28%). Relative contributions from Hg emissions in various global source regions to annual Arctic anthropogenic Hg deposition were: East Asia (32%), CIS countries (12%), Africa (12%), Europe (8%), Southeast Asia (8%), South Asia (7%), South America (7%), Central America (6%), Arctic (3%), North America (3%), Middle East (2%), and Australia and New Zealand (0.1%). Global mercury emissions from the industrial sector contributed half (48%) of the Arctic anthropogenic Hg deposition followed by contributions from ASGM (28%), power generation (17%), and the intentional use and product waste group (7%). Models estimate that global wildfire emissions are responsible for 12–17 Mg yr^{-1} of Hg deposition in the Arctic, representing 6% to 10% of annual Hg deposition in the Arctic, with wildfire contributions from Eurasia, Africa, and North America of 5.3%, 2.5%, and 1%, respectively.

The model ensemble simulates significant geographic and seasonal variations in global anthropogenic Hg deposition contributions in the Arctic, reflecting regional differences in proximity to the mid-latitude anthropogenic sources, land use, precipitation amounts, and inter-seasonal shift in atmospheric circulation and deposition pathways. Eastern High Arctic (north of 70°N) receives a relatively higher proportion of annual Hg deposition from anthropogenic sources (30% to 50%) than the western Arctic High Arctic ($\leq$ 30%). Generally, differences in relative anthropogenic Hg deposition contributions from emissions in various worldwide geographic regions to different Arctic regions are small, reflecting a long lifetime of Hg in the atmosphere. In fall and winter, there is no clear distinction in anthropogenic Hg deposition contributions between Subarctic and High Arctic regions. In springtime, anthropogenic Hg deposition contribution is exacerbated by AMDEs over sea ice resulting in the highest deposition fluxes in the High Arctic. In summer, efficient Hg uptake by vegetation in temperate and Subarctic regions and the northward retreat of the polar front limit Hg transport and deposition in the High Arctic. The Western Canadian Arctic and Eastern Siberia are more impacted by wildfires than other regions in the Arctic.

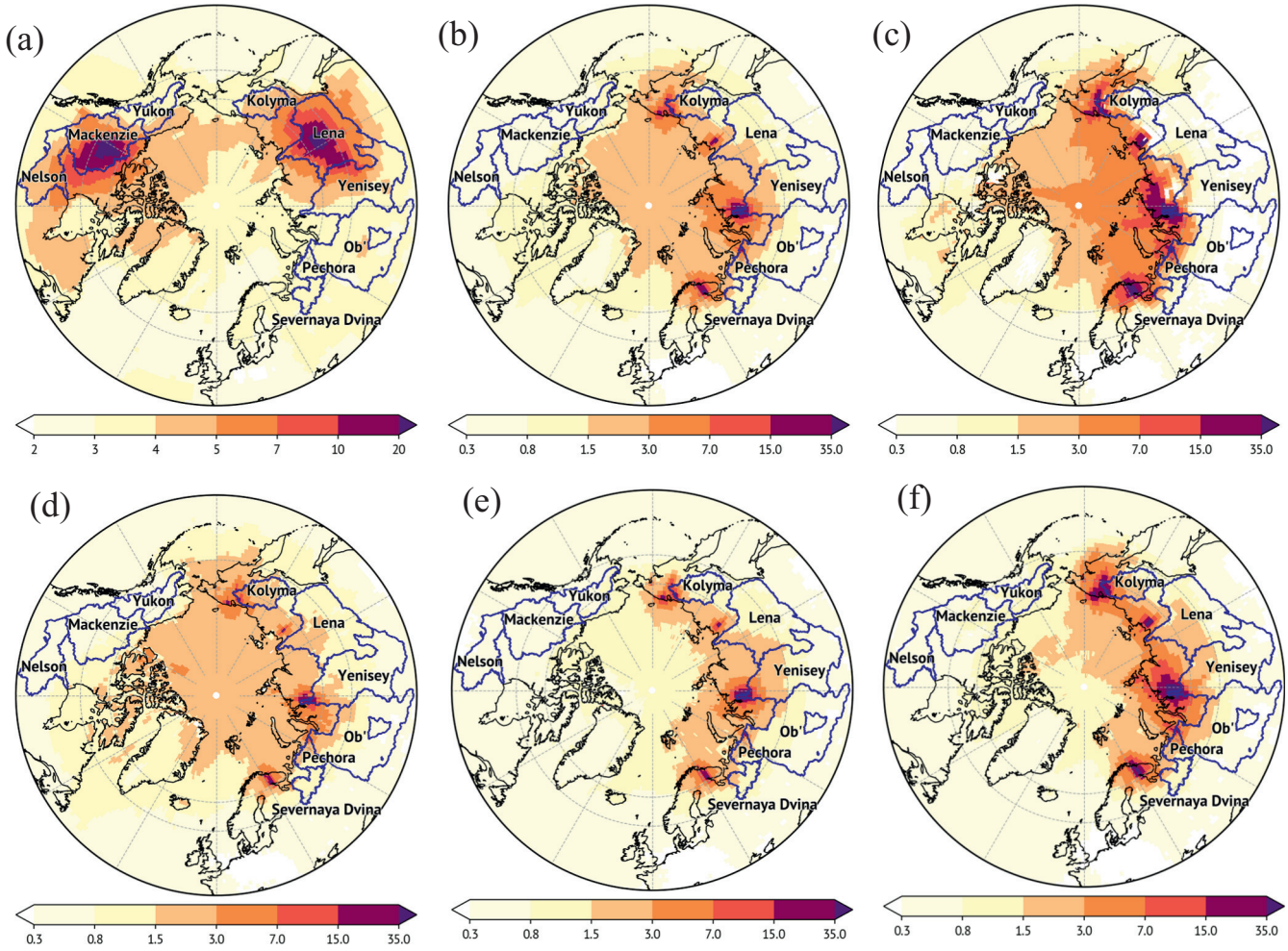

Fig. 9. GEOS-Chem simulated relative contributions of local (Arctic) wildfire Hg emissions to annual total deposition of Hg (a) in 2015. Model ensemble simulated relative contributions of local anthropogenic Hg emissions to anthropogenic Hg deposition in 2015: annual (b), winter (c), spring (d), summer (e), and fall (f).

The model ensemble estimated that anthropogenic emissions from the Arctic region account for 3% of the total (from all sources) anthropogenic Hg deposition in the Arctic. Regionally, annual Arctic region contributions to anthropogenic Hg deposition are 2% to 7% over the Arctic Ocean and up to 35% over land in Eurasia. There are notable seasonal differences in Hg deposition contributions of local anthropogenic origin. In winter and fall, efficient low-level Hg transport of north Eurasian emissions over frozen surfaces combined with inefficient removal processes lead to higher local anthropogenic contributions of 3% to 15% to the eastern Arctic Ocean and over 15% to the High Arctic terrestrial surfaces. In summer and spring, both weak transport into the Arctic polar dome and efficient wet and dry removal of Hg result in <3% contributions of local anthropogenic sources to the total anthropogenic deposition in the Arctic Ocean.

Global emission inventories, prepared in a fully documented, transparent, and consistent manner, are essential to future efforts to (globally) model mercury air transport and deposition and provide information on source-receptor relationships. The same requirements apply to their geospatial distribution. In addition to developing emissions/release estimates at the national (or sub-national) level for key emissions sectors, additional data are therefore needed to support and improve the process of assigning these emissions/releases to point sources or distributed sources. Further work is urgently needed to better define the speciation of geospatially distributed Hg emissions. Further understanding is also needed of the fate of Hg emitted as Hg(0) from ASGM activities; in particular, to determine whether these emissions are subject to long-range transport or are rapidly transformed and contribute primarily to local contamination. A better estimation of the proportion of gaseous Hg to particulate Hg and the propensity of different biomes (such as boreal peatlands) to release Hg during wildfires is needed to develop better wildfire Hg emission inventories and reduce uncertainties in modeling estimates.

Improved understanding and modeling of vegetation Hg uptake, activation of bromine species from snowpacks, and blowing snow and air-surface exchange fluxes are needed to reduce uncertainties in model simulations of atmospheric Hg in the Arctic. Additional studies are needed to improve the understanding of oxidation and reduction reactions of Hg in the gas phase as well as at environmental surfaces and aqueous environments. Model evaluation is hampered by the limited number of air concentration and wet deposition monitoring sites in the Arctic, particularly in Siberia, eastern subarctic Canada, and the Arctic Ocean. Mercury evasion fluxes from the Arctic Ocean are seasonally highly variable, but measured estimates of atmosphere-ocean Hg fluxes are only available for fall. Year-round observations are needed to evaluate modeled atmosphere-ocean Hg exchange fluxes. Fully interactive atmosphere-land-ocean biogeochemical models are needed to simulate the impacts of changing physical and biochemical environments on atmospheric Hg levels in the Arctic and explain their trends.

Declaration of competing interest

The authors declare that they have no known competing financial interests or personal relationships that could have appeared to influence the work reported in this paper.

Acknowledgments

This review is a result of efforts led by the Arctic Monitoring and Assessment Programme (AMAP) and the AMAP Mercury Expert Group to produce the 2021 AMAP Mercury Assessment. The authors thank assessment leads John Chételat (ECCC, Canada) and Rune Dietz (Aarhus University, Denmark) for their guidance, support, and technical insights on the material. Graphics production and technical editing were supported by AMAP. Institutional support for this review was provided by Environment and Climate Change Canada. The authors would like to acknowledge the efforts and contributions of all those who participated in the AMAP/UN-Environment expert groups responsible for preparing the technical background to the UN-Environment GMA 2018, and the related work to develop the AMAP/GMA global inventory of anthropogenic emissions to air in 2015. Hélène Angot acknowledges Noelle E. Selin and the use of the Svante cluster provided by the Massachusetts Institute of Technology's Joint Program on the Science and Policy of Global Change. The authors acknowledge Kenjiro Toyota and Geoff Stupple for their support with the discussion of changes in atmospheric Hg. Finally, the authors acknowledge the Atmospheric Mercury Network (AMNet), European Monitoring and Evaluation Programme (EMEP), and Environment and Climate Change Canada-Atmospheric Mercury Measurement Network (ECCC-AMM) and their contributing scientists for the provision of mercury measurement data.

CRediT authorship contribution statement

Ashu Dastoor: Conceptualization, Writing – Original Draft, Writing - Review & Editing, Modeling, Analysis. **Simon J. Wilson:** Conceptualization, Writing – Original Draft, Writing - Review & Editing, Data Curation, Analysis, Visualization. **Oleg Travnikov:** Writing – Original Draft, Modeling, Analysis, Visualization. **Andrei Ryjkov:** Writing – Original Draft, Modeling, Analysis, Visualization. **Hélène Angot:** Writing – Original Draft, Modeling, Analysis. **Jesper H. Christensen:** Modeling, Analysis. **Frits Steenhuisen:** Writing – Review & Editing, Analysis, Visualization. **Marilena Muntean:** Writing – Review & Editing.

Appendix A. Supplementary data

Supplementary data to this article can be found online at https://doi.org/10.1016/j.scitotenv.2022.156213.

References

Abbatt, J.P.D., Thomas, J.L., Abrahamsson, K., Boxe, C., Granfors, A., Jones, A.E., King, M.D., Saiz-Lopez, A., Shepson, P.B., Sodeau, J., Toohey, D.W., Toubin, C., von Glasow, R., Wren, S.N., Yang, X., 2012. Halogen activation via interactions with environmental ice and snow in the polar lower troposphere and other regions. Atmos. Chem. Phys. 12 (14), 6237–6271.

AMAP, 1998. AMAP Assessment Report: Arctic Pollution Issues. Arctic Monitoring and Assessment Programme (AMAP), Oslo, Norway. vol. xii + 859 pp.

AMAP, 2005. AMAP Assessment 2002: Heavy Metals in the Arctic. Arctic Monitoring and Assessment Programme (AMAP), Oslo, Norway (xvi + 265 pp).

AMAP, 2011. AMAP Assessment 2011: Mercury in the Arctic. Arctic Monitoring and Assessment Programme (AMAP), Oslo, Norway (xiv + 193 pp).

AMAP, 2017. Snow, Water, Ice and Permafrost in the Arctic (SWIPA) 2017. Arctic Monitoring and Assessment Programme (AMAP), Oslo, Norway (Xiv + 269 pp).

AMAP, 2021. AMAP Assessment 2021: Mercury in the Arctic. Arctic Monitoring and Assessment Programme (AMAP), Tromsø, Norway.

AMAP/UNEP, 2008. Technical Background Report to the Global Atmospheric Mercury Assessment. Arctic Monitoring and Assessment Programme / UNEP Chemicals Branch (159 pp).

AMAP/UNEP, 2013. Technical Background Report for the Global Mercury Assessment 2013. Arctic Monitoring and Assessment Programme, Oslo, Norway/UNEP Chemicals Branch, Geneva, Switzerland (vi + 263 pp).

AMAP/UNEP, 2019. Technical Background Report for the Global Mercury Assessment 2018. Arctic Monitoring and Assessment Programme, Oslo, Norway/UN Environnement Programme, Chemicals and Health Branch, Geneva, Switzerland. https://www.amap.no/documents/doc/Technical-Background-Report-for-the-Global-Mercury-Assessment-2018/1815.

Amiro, B.D., Todd, J.B., Wotton, B.M., Logan, K.A., Flannigan, M.D., Stocks, B.J., Mason, J.A., Martell, D.L., Hirsch, K.G., 2001. Direct carbon emissions from Canadian forest fires, 1959-1999. Can. J. For. Res. 31, 512–525.

Amos, H.M., Jacob, D.J., Holmes, C.D., Fisher, J.A., Wang, Q., Yantosca, R.M., Corbitt, E.S., Galarneau, E., Rutter, A.P., Gustin, M.S., Steffen, A., Schauer, J.J., Graydon, J.A., Louis, V.L. St, Talbot, R.W., Edgerton, E.S., Zhang, Y., Sunderland, E.M., 2012. Gas-particle partitioning of atmospheric hg(II) and its effect on global mercury deposition. Atmos. Chem. Phys. 12, 591–603.

Angot, H., Dastoor, A., De Simone, F., Gårdfeldt, K., Gencarelli, C.N., Hedgecock, I.M., Langer, S., Magand, O., Mastromonaco, M.N., Nordstrøm, C., Pfaffhuber, K.A., Pirrone, N., Ryjkov, A., Selin, N.E., Skov, H., Song, S., Sprovieri, F., Steffen, A., Toyota, K., Travnikov, O., Yang, X., Dommergue, A., 2016. Chemical cycling and deposition of atmospheric mercury in polar regions: review of recent measurements and comparison with models. Atmos. Chem. Phys. 16, 10735–10763. https://doi.org/10.5194/acp-16-10735-2016.

Bartels-Rausch, T., Krysztofiak, G., Bernhard, A., Schläppi, M., Schwikowski, M., Ammann, M., 2011. Photoinduced reduction of divalent mercury in ice by organic matter. Chemosphere 82 (2), 199–203.

Berg, T., Pfaffhuber, K.A., Cole, A.S., Engelsen, O., Steffen, A., 2013. Ten-year trends in atmospheric mercury concentrations, meteorological effects and climate variables at zeppelin, Ny-Ålesund. Atmos. Chem. Phys. 13, 6575–6586.

Bognar, K., Zhao, X., Strong, K., Chang, R.Y.W., Frieß, U., Hayes, P.L., McClure-Begley, A., Morris, S., Tremblay, S., Vicente-Luis, A., 2020. Measurements of tropospheric bromine monoxide over four halogen activation seasons in the Canadian high Arctic. J. Geophys. Res. Atmos. 125. https://doi.org/10.1029/2020JD033015 (e2020JD033015).

Bottenheim, J.A., Dastoor, A., Gong, S.-L., Higuchi, K., Li, Y.-F., 2004. Long range transport of air pollution to the Arctic. Inter-continental Transport of Air Pollution, the Handbook of Environmental Chemistry. vol. 4, part G, pp. 13–39.

Bougoudis, I., Blechschmidt, A.-M., Richter, A., Seo, S., Burrows, J.P., Theys, N., Rinke, A., 2020. Long-term time series of Arctic tropospheric BrO derived from UV–VIS satellite remote sensing and its relation to first-year sea ice. Atmos. Chem. Phys. 20, 11869–11892. https://doi.org/10.5194/acp-20-11869-2020.

Box, J.E., Res, E., Box, J.E., Colgan, W.T., Christensen, T.R., Schmidt, N.M., Lund, M., Parmentier, F.W.J.W., Brown, R., Bhatt, U.S., Euskirchen, E.S., Romanovsky, V.E., Walsh, J.E., Overland, J.E., Wang, M., Corell, R.W., Meier, W.N., Wouters, B., Mernild, S., Mård, J., Pawlak, J., Olsen, M.S., 2019. Key indicators of Arctic climate change: 1971–2017 Key indicators of Arctic climate change: 1971–2017. Environ. Res. Lett. 14, 045010. https://doi.org/10.1088/1748-9326/aafc1b.

Bozem, H., Hoor, P., Kunkel, D., Köllner, F., Schneider, J., Herber, A., Schulz, H., Leaitch, W.R., Aliabadi, A.A., Willis, M.D., Burkart, J., Abbatt, J.P.D., 2019. Characterization of transport regimes and the polar dome during Arctic spring and summer using in situ aircraft measurements. Atmos. Chem. Phys. 19, 15049–15071. https://doi.org/10.5194/acp-19-15049-2019.

Brooks, S.B., Saiz-Lopez, A., Skov, H., Lindberg, S.E., Plane, J.M.C., Goodsite, M.E., 2006. The mass balance of mercury in the springtime arctic environment. Geophys. Res. Lett. 33.

Bullock, D., Johnson, S., 2011. Electric Generating Utility Mercury Speciation Profiles for Clean Air Mercury Rule, EPA-454/R-11-010. EPA.

Cao, S.Z., Zhang, L., Zhang, Y., Wang, S.X., Wu, Q.R., 2022. Impacts of removal compensation effect on the mercury emission inventories for nonferrous metal (zinc, lead, and copper) smelting in China. Environ. Sci. Technol. 2022 (56), 2163–2171.

Chen, L., Liu, M., Fan, R., Ma, S., Xu, Z., Ren, M., He, Q., 2013. Mercury speciation and emission from municipal solid waste incinerators in the Pearl River Delta, South China. Sci. Total Environ. 447, 396–402.

Chen, L., Zhang, Y., Jacob, D.J., Soerensen, A.L., Fisher, J.A., Horowitz, H.M., Corbitt, E.S., Wang, X., 2015. A decline in Arctic Ocean mercury suggested by differences in decadal trends of atmospheric mercury between the Arctic and northern midlatitudes. Geophys. Res. Lett. 42, 6076–6083. https://doi.org/10.1002/2015GL064051.

Chételat, J., McKinney, M.A., Amyot, M., Dastoor, A., Douglas, T.A., Heimbürger-Boavida, L.-E., Kirk, J., Kahilainen, K.K., Outridge, P.M., Pelletier, N., Skov, H., St. Pierre, K., Vuorenmaa, J., Wang, F., 2022. Climate change and mercury in the Arctic: abiotic interactions. Sci. Total Environ. 824, 153715. https://doi.org/10.1016/j.scitotenv.2022.153715.

Christensen, J.H., Brandt, J., Frohn, L.M., Skov, H., 2004. Modelling of mercury in the Arctic with the Danish Eulerian hemispheric model. Atmos. Chem. Phys. Eur. Geosci. Union 4, 2251–2257.

Cole, A.S., Steffen, A., 2010. Trends in long-term gaseous mercury observations in the Arctic and effects of temperature and other atmospheric conditions. Atmos. Chem. Phys. 10, 4661–4672. https://doi.org/10.5194/acp-10-4661-2010.

Cole, A.S., Steffen, A., Pfaffhuber, K.A., Berg, T., Pilote, M., Poissant, L., Tordon, R., Hung, H., 2013. Ten-year trends of atmospheric mercury in the high Arctic compared to Canadian sub-Arctic and mid-latitude sites. Atmos. Chem. Phys. 13, 1535–1545. https://doi.org/10.5194/acp-13-1535-2013.

Dastoor, A.P., Durnford, D.A., 2014. Arctic Ocean: is it a sink or a source of atmospheric mercury? Environ. Sci. Technol. 48, 1707–1717. https://doi.org/10.1021/es404473e.

Dastoor, A.P., Davignon, D., Theys, N., Van Roozendael, M., Steffen, A., Ariya, P.A., 2008. Modeling dynamic exchange of gaseous elemental mercury at polar sunrise. Environ. Sci. Technol. 42, 5183–5188.

Dastoor, A., Ryzhkov, A., Durnford, D., Lehnherr, I., Steffen, A., Morrison, H., 2015. Atmospheric mercury in the Canadian Arctic. Part II: insight from modeling. Sci. Total Environ. 509–520, 16–27.

Dastoor, A., Angot, H., Bieser, J., Christensen, J.H., Douglas, T.A., Heimbürger-Boavida, L.-E., Jiskra, M., Mason, R.P., McLagan, D.S., Obrist, D., Outridge, P.M., Petrova, M.V., Ryjkov, A., St. Pierre, K.A., Schartup, A.T., Sørensen, A.L., Toyota, K., Travnikov, O., Wilson, S.J., Zdanowicz, C., 2022. Arctic mercury cycling. Natur. Rev. Earth Environ. https://doi.org/10.1038/s43017-022-00269-w.

Davini, P., Cagnazzo, C., Gualdi, S., Navarra, A., 2012. Bidimensional diagnostics, variability and trends of Northern Hemisphere blocking. J. Clim. 25, 6496–6509.

De Simone, F., Artaxo, P., Bencardino, M., Cinnirella, S., Carbone, F., D'Amore, F., Dommergue, A., Feng, X.B., Gencarelli, C.N., Hedgecock, I.M., Landis, M.S., Sprovieri,

F., Suzuki, N., Wängberg, I., Pirrone, N., 2017. Particulate-phase mercury emissions from biomass burning and impact on resulting deposition: a modeling assessment. Atmos. Chem. Phys. 17, 1881–1899.

Deeds, D.A., Banic, C.M., Lu, J., Daggupaty, S., 2013. Mercury speciation in a coal-fired power plant plume: an aircraft-based study of emissions from the 3640 MW Nanticoke Generating Station, Ontario, Canada. J. Geophys. Res. 118, 4919–4935.

Demers, J.D., Blum, J.D., Zak, D.R., 2013. Mercury isotopes in a forested ecosystem: Implications for air-surface exchange dynamics and the global mercury cycle. Glob. Biogeochem. Cycles 27, 222–238. https://doi.org/10.1002/gbc.20021.

Dibble, T.S., Tetu, H.L., Jiao, Y., Thackray, C.P., Jacob, D.J., 2020. Modeling the OH-initiated oxidation of mercury in the global atmosphere without violating physical laws. J. Phys. Chem. A 124 (2), 444–453. https://doi.org/10.1021/acs.jpca.9b10121.

Dietz, R., Outridge, P.M., Hobson, K.A., 2009. Anthropogenic contributions to mercury levels in present-day Arctic animals – a review. Sci. Total Environ. 407, 6120–6131. https://doi.org/10.1016/J.SCITOTENV.2009.08.036.

DiMento, B.P., Mason, R.P., Brook, S., Moore, C., 2019. The impact of sea ice on the air-sea exchange of mercury in the Arctic Ocean. Deep-Sea Res. I 144, 28–38. https://doi.org/10.1016/j.dsr.2018.12.001.

Dobricic, S., Vignati, E., Russo, S., 2016. Large-scale atmospheric warming in winter and the arctic sea ice retreat. J. Clim. 29, 2869–2888.

Douglas, T.A., Blum, J.D., 2019. Mercury isotopes reveal atmospheric gaseous mercury deposition directly to the Arctic coastal snowpack. Environ. Sci. Technol. Lett. https://doi.org/10.1021/acs.estlett.9b00131.

Douglas, T.A., Sturm, M., Simpson, W.R., Brooks, S., Lindberg, S.E., Perovich, D.K., 2005. Elevated mercury measured in snow and frost flowers near arctic sea ice leads. Geophys. Res. Lett. 32 (4). https://doi.org/10.1029/2004GL022132.

Douglas, T.A., Sturm, M., Simpson, W.R., Blum, J.D., Alvarez-Aviles, L., Keeler, G.J., Perovich, D.K., Biswas, A., Johnson, K., 2008. Influence of snow and ice crystal formation and accumulation on mercury deposition to the Arctic. Environ. Sci. Technol. 42, 1542–1551.

Douglas, T.A., Loseto, L.L., Macdonald, R.W., Outridge, P., Dommergue, A., Poulain, A., Amyot, M., Barkay, T., Berg, T., Chételat, J., Constant, P., Evans, M., Ferrari, C., Gantner, N., Johnson, M.S., Kirk, J., Kroer, N., Larose, C., Lean, D., Nielsen, T.G., Poissant, L., Rognerud, S., Skov, H., Sorensen, S., Wang, F.Y., Wilson, S., Zdanowicz, C.M., 2012. The fate of mercury in Arctic terrestrial and aquatic ecosystems, a review. Environ. Chem. 9, 321–355. https://doi.org/10.1071/en11140.

Douglas, T.A., Sturm, M., Blum, J.D., Polashenski, C., Stuefer, S., Hiemstra, C., Steffen, A., Filhol, S., Prevost, R., 2017. A pulse of mercury and major ions in snowmelt runoff from a small Arctic Alaska watershed. Environ. Sci. Technol. https://doi.org/10.1021/acs.est.7b03683.

Duncan, B.N., Bey, I., 2004. A modeling study of the export pathways of pollution from Europe: Seasonal and interannual variations (1987–1997). J. Geophys. Res. Atmos. 109 (D8), D08301.

Durnford, D., Dastoor, A., 2011. The behavior of mercury in the cryosphere: a review of what we know from observations. J. Geophys. Res. 116, 116.

Durnford, D., Dastoor, A., Figueras-Nieto, D., Ryjkov, A., 2010. Long range transport of mercury to the Arctic and across Canada. Atmos. Chem. Phys. 10, 6063–6086. https://doi.org/10.5194/acp-10-6063-2010.

Durnford, D., Dastoor, A., Ryzhkov, A., Poissant, L., Pilote, M., Figueras-Nieto, D., 2012. How relevant is the deposition of mercury onto snowpacks? − Part 2: a modeling study. Atmos. Chem. Phys. 12, 9251–9274. https://doi.org/10.5194/acp-12-9251-2012.

Eckhardt, S., Stohl, A., Beirle, S., Spichtinger, N., James, P., Forster, C., Junker, C., Wagner, T., Platt, U., Jennings, S.G., 2003. The North Atlantic Oscillation controls air pollution transport to the Arctic. Atmos. Chem. Phys. 3, 1769–1778. https://doi.org/10.5194/acp-3-1769-2003.

Feldstein, S.B., 2002. Fundamental mechanisms of the growth and decay of the PNA teleconnection pattern. Q.J.R. Meteorol. Soc. 128, 775–796.

Ferrari, C.P., Gauchard, P.A., Aspmo, K., Dommergue, A., Magand, O., Bahlmann, E., Nagorski, S., Temme, C., Ebinghaus, R., Steffen, A., Banic, C., Berg, T., Planchon, F., Barbante, C., Cescon, P., Boutron, C.F., 2005. Snow-to-air exchanges of mercury in an Arctic seasonal snow pack in Ny-Ålesund, Svalbard. Atmos. Environ. 39, 7633–7645. https://doi.org/10.1016/J.ATMOSENV.2005.06.058.

Finley, B.D., Swartzendruber, P.C., Jaffe, D.A., 2009. Particulate mercury emissions in regional wildfire plumes observed at the Mount Bachelor Observatory. Atmos. Environ. 43, 6074–6083.

Fisher, J.A., Jacob, D.J., Soerensen, A.L., Amos, H.M., Steffen, A., Sunderland, E.M., 2012. Riverine source of Arctic Ocean mercury inferred from atmospheric observations. Nat. Geosci. 5, 499–504.

Francis, J.A., Vavrus, S.J., Cohen, J., 2017. Amplified Arctic warming and mid-latitude weather: new perspectives on emerging connections. Wiley Interdiscip. Rev. Clim. Chang. 8, e474. https://doi.org/10.1002/wcc.474.

Fraser, A., Dastoor, A., Ryjkov, A., 2018. How important is biomass burning in Canada to mercury contamination. Atmos. Chem. Phys. 18, 7263. https://doi.org/10.5194/acp-18-7263-2018.

Friedli, H.R., Radke, L.F., Lu, J.Y., 2001. Mercury in smoke from biomass fires. Geophys. Res. Lett. 28, 3223–3226.

Friedli, H.R., Radke, L.F., Lu, J.Y., Banic, C.M., Leaitch, W.R., MacPherson, J.I., 2003a. Mercury emissions from burning of biomass from temperate North American forests: laboratory and airborne measurements. Atmos. Environ. 37, 253–267.

Friedli, H.R., Radke, L.F., Prescott, R., Hobbs, P.V., Sinha, P., 2003b. Mercury emissions from the August 2001 wildfires in Washington State and an agricultural waste fire in Oregon and atmospheric mercury budget estimates. Glob. Biogeochem. Cycles 17, 1039.

Friedli, H.R., Arellano, A., Cinnirella, S., Pirrone, N., 2009. Initial estimates of mercury emissions to the atmosphere from global biomass burning. Environ. Sci. Technol. 43, 3507–3513.

Fuelberg, H.E., Harrigan, D.L., Sessions, W., 2010. A meteorological overview of the ARCTAS 2008 mission. Atmos. Chem. Phys. 10, 817–842. https://doi.org/10.5194/acp-10-817-2010.

Gay, D.A., Schmeltz, D., Prestbo, E., Olson, M., Sharac, T., Tordon, R., 2013. The Atmospheric Mercury Network: measurement and initial examination of an ongoing atmospheric mercury record across North America. Atmos. Chem. Phys. 13, 11,339–11,349 doi: https://doi.org/10.5194/acp-13-11,339-2013.

Gerson, J.R., Szponar, N., Zambrano, A.A., Bergquist, B., Broadbent, E., Driscoll, C.T., Erkenswick, G., Evers, D.C., Fernandez, L.E., Hsu-Kim, H., Inga, G., Lansdale, K.N., Marchese, M.J., Martinez, A., Moore, C., Pan, W.K., Pérez Purizaca, R., Sánchez, V., Silman, M., Ury, E.A., Vega, C., Watsa, M., Bernhardt, E.S., 2022. Amazon forests capture high levels of atmospheric mercury pollution from artisanal gold mining. Nat. Commun. 13, 559. https://doi.org/10.1038/s41467-022-27,997-3.

Giglio, L., Randerson, J.T., van der Werf, G.R., 2013. Analysis of daily, monthly, and annual burned area using the fourth-generation global fire emissions database (GFED4). J. Geophys. Res. Biogeosci. 118, 317–328.

Goodsite, M.E., Plane, J.M.C., Skov, H., 2004. A theoretical study of the oxidation of Hg^0 to $HgBr_2$ in the troposphere. Environ. Sci. Technol. 38 (6), 1772–1776.

Hirdman, D., Burkhart, J.F., Sodemann, H., Eckhardt, S., Jefferson, A., Quinn, P.K., Sharma, S., Ström, J., Stohl, A., 2010. Long-term trends of black carbon and sulphate aerosol in the Arctic: changes in atmospheric transport and source region emissions. Atmos. Chem. Phys. 10 (19), 9351–9368.

Holmes, C.D., Jacob, D.J., Corbitt, E.S., Mao, J., Yang, X., Talbot, R., Slemr, F., 2010. Global atmospheric model for mercury including oxidation by bromine atoms. Atmos. Chem. Phys. 10 (24), 12,037–12,057. https://doi.org/10.5194/acp-10-12,037-2010.

Horowitz, H.M., Jacob, D.J., Zhang, Y., Dibble, T.S., Slemr, F., Amos, H.M., Schmidt, J.A., Corbitt, E.S., Marais, E.A., Sunderland, E.M., 2017. A new mechanism for atmospheric mercury redox chemistry: implications for the global mercury budget. Atmos. Chem. Phys. 17, 6353–6371.

IPCC 2013.

Jaffe, D., Prestbo, E., Swartzendruber, P., Weiss-Penzias, P., Kato, S., Takami, A., Hatakeyama, S., Kajii, Y., 2005. Export of atmospheric mercury from Asia. Atmos. Environ. 39, 3029–3038.

Jiao, Y., Dibble, T.S., 2015. Quality structures, vibrational frequencies, and thermochemistry of the products of reaction of BrHg. with NO2, HO2, ClO, BrO, and IO. J. Phys. Chem. A 119, 10,502–10,510.

Jiao, C., Flanner, M.G., 2016. Changing black carbon transport to the Arctic from present day to the end of 21st century. J. Geophys. Res. Atmos. 121, 4734–4750. https://doi.org/10.1002/2015JD023964.

Jiskra, M., Wiederhold, J.G., Skyllberg, U., Kronberg, R.M., Kretzschmar, R., 2017. Source tracing of natural organic matter bound mercury in boreal forest runoff with mercury stable isotopes. Environ Sci Process Impacts 19, 1235–1248.

Jiskra, M., Sonke, J.E., Obrist, D., Bieser, J., Ebinghaus, R., Myhre, C.L., Pfaffhuber, K.A., Wängberg, I., Kyllönen, K., Worthy, D., Martin, L.G., Labuschagne, C., Mkololo, T., Ramonet, M., Magand, O., Dommergue, A., 2018. A vegetation control on seasonal variations in global atmospheric mercury concentrations. Nat. Geosci. 11, 244–250.

Johnson, K.P., Blum, J.D., Keeler, G.J., Douglas, T.A., 2008. Investigation of the deposition and emission of mercury in arctic snow during an atmospheric mercury depletion event. J. Geophys. Res. Atmos. 113 (D17304). https://doi.org/10.1029/2008JD009893.

Klonecki, A., 2003. Seasonal changes in the transport of pollutants into the Arctic troposphere-model study. J. Geophys. Res. 108, 8367. https://doi.org/10.1029/2002JD002199.

Kocman, D., Wilson, S.J., Amos, H.M., Telmer, K.H., Steenhuisen, F., Sunderland, E.M., Mason, R.P., Outridge, P., Horvat, M., 2017. Toward an assessment of the global inventory of present-day mercury releases to freshwater environments. Int. J. Environ. Res. Public Health 2017 (14), 138. https://doi.org/10.3390/ijerph14020138.

Kohlenberg, A.J., Turetsky, M.R., Thompson, D.K., Branfireun, B.A., Mitchell, C.P.J., 2018. Controls on boreal peat combustion and resulting emissions of carbon and mercury. Environ. Res. Lett. 13, 035005.

Kos, G., Ryzhkov, A., Dastoor, A., Narayan, J., Steffen, A., Ariya, P.A., Zhang, L., 2013. Evaluation of discrepancy between measured and modeled oxidized mercury species. Atmos. Chem. Phys. 13, 4839–4863. https://doi.org/10.5194/acp-13-4839-2013.

Kumar, A., Wu, S., 2019. Mercury pollution in the arctic from wildfires: source attribution for the 2000s. Environ. Sci. Technol. 53, 11,269–11,275.

Kumar, A., Wu, S., Huang, Y., Liao, H., Kaplan, J.O., 2018. Mercury from wildfires: Global emission inventories and sensitivity to 2000–2050 global change. Atmos. Environ. 173, 6–15.

Kwon, S.Y., Selin, N.E., 2016. Uncertainties in atmospheric mercury modeling for policy evaluation. Curr. Pollut. Rep. 2 (2), 103–114.

Law, K.S., Stohl, A., Quinn, P.K., Brock, C.A., Burkhart, J.F., Paris, J.-D., Ancellet, G., Singh, H.B., Roiger, A., Schlager, H., Dibb, J., Jacob, D.J., Arnold, S.R., Pelon, J., Thomas, J.L., 2014. Arctic air pollution: new Insights from POLARCAT-IPY. Bull. Am. Meteorol. Soc. 95, 1873–1895. https://doi.org/10.1175/BAMS-D-13-00017.1.

Lee, M.-Y., Hong, C.-C., Hsu, H.-H., 2015. Compounding effects of warm sea surface temperature and reduced sea ice on the extreme circulation over the extratropical North Pacific and North America during the 2013–2014 boreal winter. Geophys. Res. Lett. 42, 1612–1618. https://doi.org/10.1002/2014GL062956.

Lim, A.G., Jiskra, M., Sonke, J.E., Loiko, S.V., Kosykh, N., Pokrovsky, O.S., 2020. A revised northern soil Hg pool, based on western Siberia permafrost peat Hg and carbon observations. Biogeosciences 17, 3083–3097.

Lizundia-Loiola, J., Otón, G., Ramo, R., Chuvieco, E., 2020. A spatio-temporal active-fire clustering approach for global burned area mapping at 250 m from MODIS data. Remote Sens. Environ. 236 (111), 493.

Lyman, S.N., Cheng, I., Gratz, L.E., Weiss-Penzias, P., Zhang, L., 2020. An updated review of atmospheric mercury. Sci. Total Environ. 707 (135), 575.

Mack, M.C., Bret-Harte, M.S., Hollingsworth, T.N., Jandt, R.R., Schuur, E.A.G., Shaver, G.R., Verbyla, D.L., 2011. Carbon loss from unprecedented Arctic tundra wildfire. Nature 475, 489–492.

MacMillan, G.A., Girard, C., Chételat, J., Laurion, I., Amyot, M., 2015. High methylmercury in arctic and subarctic ponds is related to nutrient levels in the warming Eastern Canadian Arctic. Environ. Sci. Technol. 49 (13), 7743–7753.

MacSween, K., Stupple, G., Aas, W., Kyllönen, K., Pfaffhuber, K.A., Skov, H., Steffen, A., Berg, T., Mastromonaco, M.N., 2022. Updated trends for atmospheric mercury in the Arctic: 1995–2018. Sci. Total Environ. 837, 155802. https://doi.org/10.1016/J.SCITOTENV.2022.155802.

McLagan, D.S., Stupple, G.W., Darlington, A., Hayden, K., Steffen, A., 2021. Where there is smoke there is mercury: assessing boreal forest fire mercury emissions using aircraft and highlighting uncertainties associated with upscaling emissions estimates. Atmos. Chem. Phys. 21, 5635–5653.

Meredith, M., Sommerkorn, M., Cassotta, S., Derksen, C., Ekaykin, A., Hollowed, A., Kofinas, G., Mackintosh, A., Melbourne-Thomas, J., Muelbert, M.M.C., Ottersen, G., Pritchard, H. and Shuur, E.A.G, 2019. Polar regions In: IPCC Special Report on the Ocean and Cryosphere in a Changing Climate, Pörtner, H.-O., Roberts, D.C., Masson-Delmotte, V., Zhai, P., Tignor, M., Poloczanska, E., Mintenbeck, K., Alegría, A., Nicolai, M., Okem, A., Petzold, J., Rama, B. and Weyer, N.M. (Eds.), pp. 203–320. Intergovernmental Panel on Climate Change (IPCC). pp. 203–320 (In Press).

Mernild, S.H., Hanna, E., Mcconnell, J.R., Sigl, M., Beckerman, A.P., Yde, J.C., Cappelen, J., Malmros, J.K., Steffen, K., 2015. Greenland precipitation trends in a long-term instrumental climate context (1890–2012): evaluation of coastal and ice core records. Int. J. Climatol. 35, 303–320. https://doi.org/10.1002/JOC.3986.

Milner, A.M., Khamis, K., Battin, T.J., Brittain, J.E., Barrand, N.E., Füreder, L., Cauvy-Fraunié, S., Gíslason, G.M., Jacobseni, D., Hannaha, D.M., Hodson, A.J., Hood, E., Lencioni, V., Ólafsson, J.S., Robinson, C.T., Tranter, M., Brown, L.E., 2017. Glacier shrinkage driving global changes in downstream systems. Proc. Natl. Acad. Sci. 114 (37), 9770–9778.

Monks, S.A., Arnold, S.R., Emmons, L.K., Law, K.S., Turquety, S., Duncan, B.N., Flemming, J., Huijnen, V., Tilmes, S., Langner, J., Mao, J., Long, Y., Thomas, J.L., Steenrod, S.D., Raut, J.C., Wilson, C., Chipperfield, M.P., Diskin, G.S., Weinheimer, A., Schlager, H., Ancellet, G., 2015. Multi-model study of chemical and physical controls on transport of anthropogenic and biomass burning pollution to the Arctic. Atmos. Chem. Phys. 15, 3575–3603. https://doi.org/10.5194/acp-15-3575-2015.

Moore, C.W., Obrist, D., Steffen, A., Staebler, R.M., Douglas, T.A., Richter, A., Nghiem, S.V., 2014. Convective forcing of mercury and ozone in the Arctic boundary layer induced by leads in sea ice. Nat. 2014 5,067,486 506. pp. 81–84. https://doi.org/10.1038/nature12924.

Moran, M.D., Dastoor, A., Morneau, G., 2014. Chapter 4. Long-range transport of air pollutants and regional and global air quality modeling. Air Quality Management, Canadian Perspective on a Global Issue. Springer, pp. 68–98. https://doi.org/10.1007/978-94-007-7557-2_4.

Muntean, M., Janssens-Maenhout, G., Song, S., Giang, A., Selin, N.E., Zhong, H., Zhao, Y., Olivier, J.G.J., Guizzardi, D., Crippa, M., Schaaf, E., Dentener, F., 2018. Evaluating EDGARv4.tox2 speciated mercury emissions ex-post scenarios and their impacts on modeled global and regional wet deposition patterns. Atmos. Environ. 184, 56–68.

NOAA, 2020. Climate Variability: North Atlantic Oscillation | NOAA Climate.Gov. https://www.climate.gov/news-features/understanding-climate/climate-variability-north-atlantic-oscillation.

Obrist, D., Hallar, A.G., McCubbin, I., Stephens, B.B., Rahn, T., 2008. Atmospheric mercury concentrations at Storm Peak Laboratory in the Rocky Mountains: evidence for long-range transport from Asia, boundary layer contributions, and plant mercury uptake. Atmos. Environ. 42, 7579–7589.

Obrist, D., Agnan, Y., Jiskra, M., Olson, C.L., Colegrove, D.P., Hueber, J., Moore, C.W., Sonke, J.E., Helmig, D., 2017. Tundra uptake of atmospheric elemental mercury drives Arctic mercury pollution. Nature 547, 201–204. https://doi.org/10.1038/nature22997.

Octaviani, M., Stemmler, I., Lammel, G., Graf, H.F., 2015. Atmospheric transport of persistent organic pollutants to and from the arctic under present-day and future climate. Environ. Sci. Technol. 49, 3593–3602. https://doi.org/10.1021/ES505636G/SUPPL_FILE/ES505636G_SI_001.PDF.

Olson, C.L., Jiskra, M., Sonke, J.E., Obrist, D., 2019. Mercury in tundra vegetation of Alaska: spatial and temporal dynamics and stable isotope patterns. Sci. Total Environ. 660, 1502–1512.

Osterwalder, S., Dunham-Cheatham, S.M., Ferreira, Araujo B., Magand, O., Thomas, J.L., Baladima, F., et al., 2021. Fate of springtime atmospheric reactive mercury: concentrations and deposition at Zeppelin, Svalbard. ACS Earth Space Chem. 5, 3234–3246.

Outridge, P.M., Mason, R.P., Wang, F., Guerrero, S., Heimbürger-Boavida, L.E., 2018. Updated global and oceanic mercury budgets for the United Nations Global Mercury Assessment 2018. Environ. Sci. Technol. 52, 11,466–11,477. https://doi.org/10.1021/acs.est.8b01246.

Pacyna, E.G., Pacyna, J.M., 2002. Global emission of mercury from anthropogenic sources in 1995. Water Air Soil Pollut. 137 (149–165), 2002. https://doi.org/10.1023/A:1015502430561.

Pacyna, J.M., Pacyna, E.G., Steenhuisen, F., Wilson, S., 2003. Mapping 1995 global anthropogenic emissions of mercury. Atmos. Environ. 01/2003. https://doi.org/10.1016/S1352-2310(03)00239-5.

Pacyna, E.G., Pacyna, J.M., Steenhuisen, F., Wilson, S., 2006. Global anthropogenic mercury emission inventory for 2000. Atmos. Environ. 40, 4048–4063.

Pacyna, E.G., Pacyna, J.M., Sundseth, K., Munthe, J., Kindbom, K., Wilson, S., Steenhuisen, F., Maxson, P., 2010. Global emission of mercury to the atmosphere from anthropogenic sources in 2005 and projections to 2020. Atmos. Environ. 01/2010.

Pal, B., Ariya, P.A., 2004. Studies of ozone initated reactions of gaseous mercury: kinetics, product studies, and atmospheric implications. Phys. Chem. Chem. Phys. 10, 572–578. https://doi.org/10.1039/b801226a.

Paris, J.-D., Stohl, A., Nédélec, P., Arshinov, M.Yu., Panchenko, M.V., Shmargunov, V.P., Law, K.S., Belan, B.D., Ciais, P., 2009. Wildfire smoke in the Siberian Arctic in summer: source characterization and plume evolution from airborne measurements. Atmos. Chem. Phys. 9, 9315–9327. https://doi.org/10.5194/acp-9-9315-2009.

Park, K.S., Seo, Y.C., Lee, S.J., Lee, J.H., 2008. Emission and speciation of mercury from various combustion sources. Powder Technol. 180, 151–156.

Pearson, C., Howard, D., Moore, C., Obrist, D., 2019. Mercury and trace metal wet deposition across five stations in Alaska: controlling factors, spatial patterns, and source regions. Atmos. Chem. Phys. 19 (10), 6913–6929. https://doi.org/10.5194/acp-19-6913-2019.

Pelletier, N., Chételat, J., Blarquez, O., Vermaire, J.C., 2020. Paleolimnological assessment of wildfire-derived atmospheric deposition of trace metal(loid)s and major ions to subarctic lakes (Northwest Territories, Canada). J. Geophys. Res. Biogeosci. 125, e2020JG005720.

Peterson, K.A., Shepler, B.C., Singleton, J.M., 2007. The group 12 metal chalcogenides: an accurate multireference configuration interaction and coupled cluster study. Mol. Phys. 105 (9), 1139–1155. https://doi.org/10.1080/00268970701241664.

Peterson, D.A., Campbell, J.R., Hyer, E.J., Fromm, M.D., Kablick, G.P., Cossuth, J.H., DeLand, M.T., 2018. Wildfire-driven thunderstorms cause a volcano-like stratospheric injection of smoke. Clim. Atmos. Sci. 11 (1), 1–8. https://doi.org/10.1038/s41612-018-0039-3.

Pistone, K., Eisenman, I., Ramanathan, V., 2014. Observational determination of albedo decrease caused by vanishing Arctic sea ice. Proc. Natl. Acad. Sci. U. S. A. 111, 3322–3326. https://doi.org/10.1073/PNAS.1318201111.

Pithan, F., Svensson, G., Caballero, R., Chechin, D., Cronin, T.W., Ekman, A.M.L., Neggers, R., Shupe, M.D., Solomon, A., Tjernström, M., Wendisch, M., 2018. Role of air-mass transformations in exchange between the Arctic and mid-latitudes. Nat. Geosci. 11, 805–812. https://doi.org/10.1038/s41561-018-0234-1.

Pöhler, D., Vogel, L., Frieß, U., Platt, U., 2010. Observation of halogen species in the Amundsen Gulf, Arctic, by active long-path differential optical absorption spectroscopy. Proc. Natl. Acad. Sci. 107, 6582–6587. https://doi.org/10.1073/pnas.0912231107.

Pozzoli, L., Dobricic, S., Russo, S., Vignati, E., 2017. Impacts of large-scale atmospheric circulation changes in winter on black carbon transport and deposition to the Arctic. Atmos. Chem. Phys. 17, 11,803–11,818. https://doi.org/10.5194/acp-17-11,803-2017.

Rutter, A.P., Shakya, K.M., Lehr, R., Schauer, J.J., Griffin, R.J., 2012. Oxidation of gaseous elemental mercury in the presence of secondary organic aerosols. Atmos. Environ. 59, 86–92. https://doi.org/10.1016/j.atmosenv.2012.05.009.

Saiz-Lopez, A., Sitkiewicz, S.P., Roca-Sanjuán, D., Oliva-Enrich, J.M., Dávalos, J.Z., Notario, R., Jiskra, M., Xu, Y., Wang, F., Thackray, C.P., Sunderland, E.M., Jacob, D.J., Travnikov, O., Cuevas, C.A., Acuna, A.U., Rivero, D., Plane, J.M.C., Kinnison, D.E., Sonke, J.E., 2018. Photoreduction of gaseous oxidized mercury changes global atmospheric mercury speciation, transport and deposition. Nat. Commun. 9 (1), 4796. https://doi.org/10.1038/s41467-018-07075-3.

Saiz-Lopez, A., Ulises Acuña, A., Trabelsi, T., Carmona-García, J., Dávalos, J., Z., Rivero, D., Cuevas, C.A., Kinnison, D.E., Sitkiewicz, S.P., Roca-Sanjuan, D., Francisco, J.S., 2019. Gas-phase photolysis of Hg(I) radical species: a new atmospheric mercury reduction process. J. Am. Chem. Soc. 141 (22), 8698–8702. https://doi.org/10.1021/jacs.9b02890.

Saiz-Lopez, A., Travnikov, O., Sonke, J.E., Thackray, C.P., Jacob, D.J., Carmona-García, J., Francés-Monerris, A., Roca-Sanjuán, D., Ulises Acuña, A., Dávalos, J.Z., Cuevas, C.A., Jiskra, M., Wang, F., Bieser, J., Plane, J.M.-C., Francisco, J.S., 2020. Photochemistry of oxidized Hg(I) and Hg(II) species suggests missing mercury oxidation in the troposphere. Proc. Natl. Acad. Sci. 117, 30,949–30,956.

Saros, J.E., Anderson, N.J., Juggins, S., McGowan, S., Yde, J.C., Telling, J., Bullard, J.E., Yallop, M.L., Heathcote, A.J., Burpee, B.T., Fowler, R.A., Barry, C.D., Northington, R.M., Osburn, C.L., Pla-Rabes, S., Mernild, S.H., Whiteford, E.J., Grace Andrews, M., Kerby, J.T., Post, E., 2019. Arctic climate shifts drive rapid ecosystem responses across the West Greenland landscape. Environ. Res. Lett. 14, 074027. https://doi.org/10.1088/1748-9326/AB2928.

Schartup, A.T., Soerensen, A.L., Angot, H., Bowman, K., Selin, N.E., 2022. What are the likely changes in mercury concentration in the Arctic atmosphere and ocean under future emissions scenarios? Sci. Total Environ. 836, 155477. https://doi.org/10.1016/J.SCITOTENV.2022.155477.

Schuster, P.F., Schaefer, K.M., Aiken, G.R., Antweiler, R.C., Dewild, J.F., Gryziec, J.D., Gusmeroli, A., Hugelius, G., Jafarov, E., Krabbenhoft, D.P., Liu, L., Herman-Mercer, N., Mu, C., Roth, D.A., Schaefer, T., Striegl, R.G., Wickland, K.P., Zhang, T., 2018. Permafrost stores a globally significant amount of mercury. Geophys. Res. Lett. 45, 1463–1471. https://doi.org/10.1002/2017GL075571.

Screen, J.A., Simmonds, I., 2010. The central role of diminishing sea ice in recent Arctic temperature amplification. Nat. 2010 4,647,293 464, pp. 1334–1337 https://doi.org/10.1038/nature09051.

Seager, R., Haibo, L.I.U., Kushnir, Y., Osborn, T.J., Simpson, I.R., Kelley, C.R., Nakamura, J., 2020. Mechanisms of winter precipitation variability in the European–Mediterranean Region associated with the North Atlantic Oscillation. J. Clim. 33, 7179–7196. https://doi.org/10.1175/JCLI-D-20-0011.1.

Selin, N.E., Jacob, D.J., Yantosca, R.M., Strode, S., Jaeglé, L., Sunderland, E.M., 2008. Global 3-D land-ocean atmosphere model for mercury: present-day versus preindustrial cycles and anthropogenic enrichment factors for deposition. Glob. Biogeochem. Cycles 22. https://doi.org/10.1029/2007GB003040.

Selyuzhenok, V., Bashmachnikov, I., Ricker, R., Vesman, A., Bobylev, L., 2020. Sea ice volume variability and water temperature in the Greenland Sea. Cryosphere 14, 477–495. https://doi.org/10.5194/tc-14-477-2020.

Seo, S., Richter, A., Blechschmidt, A.-M., Bougoudis, I., Burrows, J.P., 2020. Spatial distribution of enhanced BrO and its relation to meteorological parameters in Arctic and Antarctic sea ice regions. Atmos. Chem. Phys. 20, 12,285–12,312. https://doi.org/10.5194/acp-20-12,285-2020.

Serreze, M.C., Barry, R.G., 2011. Processes and impacts of Arctic amplification: a research synthesis. Glob. Planet. Chang. 77, 85–96. https://doi.org/10.1016/J.GLOPLACHA.2011.03.004.

Sharma, S., Ishizawa, M., Chan, D., Lavoué, D., Andrews, E., Eleftheriadis, K., Maksyutov, S., 2013. 16-year simulation of Arctic black carbon: transport, source contribution, and sensitivity analysis on deposition. J. Geophys. Res. Atmos. 118, 943–964. https://doi.org/10.1029/2012JD017774.

Simpson, W.R., Brown, S.S., Saiz-Lopez, A., Thornton, J.A., von Glasow, R., 2015. Tropospheric halogen chemistry: sources, cycling, and impacts. Chem. Rev. 115, 4035–4062.

Skov, H., Brooks, S.B., Goodsite, M.E., Lindberg, S.E., Meyers, T.P., Landis, M.S., Larsen, M.R., Jensen, B., McConville, G., Christensen, J., 2006. Fluxes of reactive gaseous mercury measured with a newly developed method using relaxed eddy accumulation. Atmos. Environ. 40 (5542–5463).

Skov, H., Hjorth, J., Nordstrøm, C., Jensen, B., Christoffersen, C., Bech Poulsen, M., Baldtzer Liisberg, J., Beddows, D., Dall'Osto, M., Christensen, J., 2020. The variability in gaseous elemental mercury at Villum Research Station, Station Nord in North Greenland from 1999 to 2017. Atmos. Chem. Phys. 20, 13,253–13,265. https://doi.org/10.5194/acp-20-13,253-2020.

Spicer, C.W., Sumner, A.L., Satola, J., Mangaraj, R., 2005. Kinetics of mercury reactions in the atmosphere. Report to the Florida Department of Environmental Conservation on Florida DEP Contract No. AQ192.

Sprovieri, F., Pirrone, N., Bencardino, M., D'Amore, F., Angot, H., Barbante, C., Brunke, E.G., Arcega-Cabrera, F., Cairns, W., Comero, S., Del Carmen Diéguez, M., Dommergue, A., Ebinghaus, R., Bin Feng, X., Fu, X., Elizabeth Garcia, P., Manfred Gawlik, B., Hageström, U., Hansson, K., Horvat, M., Kotnik, J., Labuschagne, C., Magand, O., Martin, L., Mashyanov, N., Mkololo, T., Munthe, J., Obolkin, V., Ramirez Islas, M., Sena, F., Somerset, V., Spandow, P., Vardè, M., Walters, C., Wängberg, I., Weigelt, A., Yang, X., Zhang, H., 2017. Five-year records of mercury wet deposition flux at GMOS sites in the Northern and Southern hemispheres. Atmos. Chem. Phys. 17, 2689–2708. https://doi.org/10.5194/ACP-17-2689-2017.

St. Louis, V.L., Sharp, M.J., Steffen, A., May, A., Barker, J., Kirk, J.L., Kelly, D.J., Arnott, S.E., Keatley, B., Smol, J.P., 2005. Some sources and sinks of monomethyl and inorganic mercury on Ellesmere Island in the Canadian High Arctic. Environ. Sci. Technol. 39 (8), 2686–2701.

Steenhuisen, F., Wilson, S.J., 2015. Identifying and characterizing major emission point sources as a basis for geospatial distribution of mercury emissions inventories. Atmos. Environ. 112, 167–177 (ISSN 1352–2310).

Steenhuisen, F., Wilson, S.J., 2019. Development and application of an updated geospatial distribution model for gridding 2015 global mercury emissions. Atmos. Environ. 211, 138–150.

Steffen, A., Schroeder, W., Macdonald, R., Poissant, L., Konoplev, A., 2005. Mercury in the Arctic atmosphere: an analysis of eight years of measurements of GEM at Alert (Canada) and a comparison with observations at Amderma (Russia) and Kuujjuarapik (Canada). Sci. Total Environ. 342, 185–198.

Steffen, A., Douglas, T., Amyot, M., Ariya, P., Aspmo, K., Berg, T., Bottenheim, J., Brooks, S., Cobbett, F., Dastoor, A., Dommergue, A., Ebinghaus, R., Ferrari, C., Gardfeldt, K., Goodsite, M.E., Lean, D., Poulain, A.J., Scherz, C., Skov, H., Sommar, J., Temme, C., 2008. A synthesis of atmospheric mercury depletion event chemistry in the atmosphere and snow. Atmos. Chem. Phys. 8, 1445–1482.

Steffen, A., Bottenheim, J., Cole, A., Douglas, T.A., Ebinghaus, R., Friess, U., Netcheva, S., Nghiem, S., Sihler, H., Staebler, R., 2013. Atmospheric mercury over sea ice during the OASIS-2009 campaign. Atmos. Chem. Phys. 13, 7007–7021. https://doi.org/10.5194/acp-13-7007-2013.

Steffen, A., Bottenheim, J., Cole, A., Ebinghaus, R., Lawson, G., Leaitch, W.R., 2014. Atmospheric mercury speciation and mercury in snow over time at Alert, Canada. Atmos. Chem. Phys. 14, 2219–2231.

Stephens, C.R., Shepson, P.B., Steffen, A., Bottenheim, J.W., Liao, J., Huey, L.G., Apel, E., Weinheimer, A., Hall, S.R., Cantrell, C., Sive, B.C., Knapp, D.J., Montzka, D.D., Hornbrook, R.S., 2012. The relative importance of chlorine and bromine radicals in the oxidation of atmospheric mercury at Barrow, Alaska. J. Geophys. Res. 117, D00R11.

Stohl, A., 2006. Characteristics of atmospheric transport into the Arctic troposphere. J. Geophys. Res. 111, D11306. https://doi.org/10.1029/2005JD006888.

Streets, D.G., Horowitz, H.M., Lu, L., Levin, L., Thackray, C.P., Sunderland, E.M., 2019a. Global and regional trends in mercury emissions and concentrations, 2010–2015. Atmos. Environ. 201, 417–427. https://doi.org/10.1016/j.atmosenv.2018.12.031.

Streets, D.G., Horowitz, H.M., Lu, Z., Levin, L., Thackray, C.P., Sunderland, E.M., 2019b. Five hundred years of anthropogenic mercury: Spatial and temporal release profiles. Environ. Res. Lett. 14.

Subir, M., Ariya, P.A., Dastoor, A.P., 2011. A review of uncertainties in atmospheric modeling of mercury chemistry I. Uncertainties in existing kinetic parameters - Fundamental limitations and the importance of heterogeneous chemistry. Atmos. Environ. 45 (32), 5664–5676.

Subir, M., Ariya, P.A., Dastoor, A.P., 2012. A review of the sources of uncertainties in atmospheric mercury modeling II. Mercury surface and heterogeneous chemistry – a missing link. Atmos. Environ. 46, 1–10.

Swanson, W.F., Graham, K.A., Halfacre, J.W., Holmes, C.D., Shepson, P.B., Simpson, W.R., 2020. Arctic reactive bromine events occur in two distinct sets of environmental conditions: a statistical analysis of 6 years of observations. J. Geophys. Res. Atmos. 125. https://doi.org/10.1029/2019JD032139 (e2019JD032139).

Tørseth, K., Aas, W., Breivik, K., Fjæraa, A.M., Fiebig, M., Hjellbrekke, A.G., Lund Myhre, C., Solberg, S., Yttri, K.E., 2012. Introduction to the European Monitoring and Evaluation Programme (EMEP) and observed atmospheric composition change during 1972–2009. Atmos. Chem. Phys. 12, 5447–5481. https://doi.org/10.5194/acp-12-5447-2012.

Toyota, K., Dastoor, A.P., Ryzhkov, A., 2014. Air-snowpack exchange of bromine, ozone and mercury in the springtime Arctic simulated by the 1-D model PHANTAS-Part 2: mercury and its speciation. Atmos. Chem. Phys. 14 (8), 4135–4167. https://doi.org/10.5194/acp-14-4135-2014.

Travnikov, O., Ilyin, I., 2009. The EMEP/MSC-E mercury modeling system. In: Mason, R., Pirrone, N. (Eds.), Mercury Fate and Transport in the Global Atmosphere: Emissions. Measurements and Models. Springer US, Boston, MA, pp. 571–587.

Travnikov, O., Angot, H., Artaxo, P., Bencardino, M., Bieser, J., D'Amore, F., Dastoor, A., De Simone, F., DIéguez, M.C., Dommergue, A., Ebinghaus, R., Bin Feng, X., Gencarelli, C.N., Hedgecock, I.M., Magand, O., Martin, L., Matthias, V., Mashyanov, N., Pirrone, N., Ramachandran, R., Alana Read, K., Ryjkov, A., Selin, N.E., Sena, F., Song, S., Sprovieri, F., Wip, D., Wängberg, I., Yang, X., 2017. Multi-model study of mercury dispersion in the atmosphere: atmospheric processes and model evaluation. Atmos. Chem. Phys. 17, 5271–5295. https://doi.org/10.5194/ACP-17-5271-2017.

UNEP, 2013. Global Mercury Assessment 2013: Sources, Emissions. Releases and Environmental Transport, UNEP Chemicals Branch, Geneva, Switzerland.

UNEP, 2019. Global Mercury Assessment 2018. UN-Environment Programme, Chemicals and Health Branch, Geneva, Switzerland (59 pp).

Veira, A., Lasslop, G., Kloster, S., 2016. Wildfires in a Warmer Climate: Emission Fluxes, Emission Heights, and Black Carbon Concentrations in 2090–2099.

Walker, X.J., Baltzer, J.L., Cumming, S.G., Day, N.J., Ebert, C., Goetz, S., Johnstone, J.F., Potter, S., Rogers, B.M., Schuur, E.A.G., Turetsky, M.R., Mack, M.C., 2019. Increasing wildfires threaten historic carbon sink of boreal forest soils. Nature 572, 520–523.

Wang, S.X., Zhang, L., Li, G.H., Wu, Y., Hao, J.M., Pirrone, N., Sprovieri, F., Ancora, M.P., 2010. Mercury emission and speciation of coal-fired power plants in China. Atmos. Chem. Phys. 10, 1183–1192. https://doi.org/10.5194/acp-10-1183-2010.

Wang, F., Pucko, M., Stern, G., 2017. Transport and transformation of contaminants in sea ice. Chapter 19, Sea Ice. Third edition. Edited by David N. Thomas. John Wiley & Sons, Ltd.

Wang, S., McNamara, S.M., Moore, C.W., Obrist, D., Steffen, A., Shepson, P.B., Staebler, R.M., Raso, A.R.W., Pratt, K.A., 2019. Direct detection of atmospheric atomic bromine leading to mercury and ozone depletion. Proc. Natl. Acad. Sci. U. S. A. 116 (29), 14,479–14,484. https://doi.org/10.1073/pnas.1900613116.

Wang, X., Luo, J., Yuan, W., Lin, C.J., Wang, F., Liu, C., Wang, G., Feng, X., 2020. Global warming accelerates uptake of atmospheric mercury in regions experiencing glacier retreat. Proc. Natl. Acad. Sci. U. S. A. 117 (4), 2049–2055. https://doi.org/10.1073/pnas.1906930117 (Epub 2020 Jan 13. PMID: 31932430; PMCID: PMC6995023).

Weigelt, A., Slemr, F., Ebinghaus, R., Pirrone, N., Bieser, J., Bödewadt, J., Esposito, G., van Velthoven, P.F.J., 2016. Mercury emissions of a coal-fired power plant in Germany. Atmos. Chem. Phys. 16, 13,653–13,668. https://doi.org/10.5194/acp-16-13,653-2016.

Weiss-Penzias, P., Jaffe, D., Swartzendruber, P., Hafner, W., Chand, D., 2007. Quantifying Asian and biomass burning sources of mercury using the Hg/CO ratio in pollution plumes observed at the Mount Bachelor Observatory. Atmos. Environ. 41, 4366–4379.

Willis, M.D., Bozem, H., Kunkel, D., Lee, A.K.Y., Schulz, H., Burkart, J., Aliabadi, A.A., Herber, A.B., Leaitch, W.R., Abbatt, J.P.D., 2019. Aircraft-based measurements of High Arctic springtime aerosol show evidence for vertically varying sources, transport and composition. Atmos. Chem. Phys. 19, 57–76. https://doi.org/10.5194/acp-19-57-2019.

Wilson, S.J., Steenhuisen, F., Pacyna, J.M., Pacyna, E.G., 2006. Mapping the spatial distribution of global anthropogenic mercury atmospheric emission inventories. Atmos. Environ. 40 (2006), 4621e4632.

Wohlgemuth, L., Osterwalder, S., Joseph, C., Kahmen, A., Hoch, G., Alewell, C., Jiskra, M., 2020. A bottom-up quantification of foliar mercury uptake fluxes across Europe. Biogeosciences 17, 6441–6456. https://doi.org/10.5194/bg-17-6441-2020.

Wu, Q.R., Wang, S.X., Zhang, L., Song, J.X., Yang, H., Meng, Y., 2012. Update of mercury emissions from China's primary zinc, lead and copper smelters, 2000–2010. Atmos. Chem. Phys. 12 (22), 11153–11,163.

Wu, X., Yang, H., Waugh, D.W., Orbe, C., Tilmes, S., Lamarque, J.-F., 2018. Spatial and temporal variability of interhemispheric transport times. Atmos. Chem. Phys. 18, 7439–7452. https://doi.org/10.5194/acp-18-7439-2018.

Yan, X., Konopka, P., Hauck, M., Podglajen, A., Ploeger, F., 2021. Asymmetry and pathways of inter-hemispheric transport in the upper troposphere and lower stratosphere. Atmos. Chem. Phys. 21, 6627–6645. https://doi.org/10.5194/acp-21-6627-2021.

Yang, Z., Fang, W., Lu, X., Sheng, G.-P., Graham, D.E., Liang, L., Wullschleger, S.D., Gu, B., 2016. Warming increases methylmercury production in an Arctic soil. Environ. Pollut. 214, 504–509.

Zhang, L., Wang, S., Wang, L., Wu, Y., Duan, L., Wu, Q., Wang, F., Yang, M., Yang, H.B., Hao, J., Liu, X., 2015. Updated emission inventories for speciated atmospheric mercury from anthropogenic sources in China. Environ. Sci. Technol. 49 (5), 3185–3194.

Zhang, L., Wang, S., Wu, Q., Wang, F., Lin, C.-J., Zhang, L., Hui, M., Yang, M., Su, H., Hao, J., 2016. Mercury transformation and speciation in flue gases from anthropogenic emission sources: a critical review. Atmos. Chem. Phys. 16, 2417–2433. https://doi.org/10.5194/acp-16-2417-2016.

Zhou, J., Obrist, D., Dastoor, A., Jiskra, M., Ryjkov, A., 2021. Vegetation uptake of mercury and impacts on global cycling. Nat. Rev. Earth Environ. 2, 269–284. https://doi.org/10.1038/s43017-021-00146-y.

Zolkos, S., Krabbenhoft, D.P., Suslova, A., Tank, S.E., McClelland, J.W., Spencer, R.G.M., Shiklomanov, A., Zhulidov, A.V., Gurtovaya, T., Zimov, N., Zimov, S., Mutter, E.A., Kutny, L., Amos, E., Holmes, R.M., 2020. Mercury export from Arctic Great Rivers. Environ. Sci. Technol. 54, 4140–4148.